

Scientific paper

# Comparison of Kinetics of Adsorption of Permanganate on Co-Al-Layered Double Hydroxide and MoS<sub>2</sub> Nanocompounds

Shahin Ghobadi, Babak Samiey, \*\* Enis Esmaili and Chil-Hung Cheng<sup>2</sup>

<sup>1</sup> Department of Chemistry, Faculty of Science, Lorestan University, Khoramabad 68137-17133, Lorestan, Iran

<sup>2</sup> Department of Chemical Engineering, Toronto Metropolitan University, Toronto, Ontario, M5B 2K3, Canada

\* Corresponding author: E-mail: babsamiey@yahoo.com, samiey.b@lu.ac.ir

Received: 11-29-2022

#### Abstract

Permanganate ( $MnO_4^-$ ) ions were adsorbed on carbonate intercalated Co-Al-layered double hydroxide (Co-Al-LDH) and  $MoS_2$  and after a while the adsorbed  $MnO_4^-$  ions were reduced to  $MnO_2$ . Reduction of adsorbed  $MnO_4^-$  ion was catalyzed on the surface of carbonate intercalated Co-Al-LDH but  $MnO_4^-$  ions reacted with  $MoS_2$  surface. Adsorption kinetic tests were carried out at different temperatures, ionic strengths, pH, initial adsorbate concentrations and shaking rates. The adsorption kinetics was studied by the kinetics of adsorption study in the regions with constant adsorption acceleration (KASRA) model and KASRA, ideal-second-order (ISO), intraparticle diffusion, Elovich and (non-ideal process of adsorption kinetics (NIPPON) equations.

In this work, a new equation called NIPPON equation was introduced. In this equation, it was assumed that during a non-ideal process, adsorbate species molecules were adsorbed simultaneously on the same type adsorption sites with different activities. Indeed, the average values of adsorption kinetic parameters were calculated by the NIPPON equation. Also, the character of boundaries of regions obtained from the KASRA model can be determined by this equation.

Keywords Co-Al-LDH, MoS<sub>2</sub>, potassium permanganate, adsorption, NIPPON equation, KASRA model

#### 1. Introduction

Industrial wastewaters, especially produced by chemical and pharmaceutical, leather, cosmetics, fabrics factories often include substances like organic synthetic substances, inorganic compounds and heavy metals that need to be treated before being discharged into the environment. There are different methods for treatment of these wastewaters such as coagulation and flocculation, filtration, sludge drying, sedimentation and adsorption. Among them, adsorption process is commonly used in industry for compound separation and wastewater treatment. This technology is especially featured by cost effectiveness and ease of design and operation.

Potassium permanganate (KMnO<sub>4</sub>) is a strong oxidizing agent and there were a few work in relation to its adsorption from aqueous media. In continuation of our earlier works,  $^{1,2}$  mechanisms of adsorption kinetics of MnO<sub>4</sub> on Co-Al-LDH and MoS<sub>2</sub> nanocompounds were studied by the KASRA model and the KASRA, ISO, NIP-PON, Elovich and intraparticle diffusion equations. MnO<sub>4</sub>

ion was adsorbed on the surface of Co-Al-LDH and MoS2 and then was reduced to MnO2 and the reaction obeyed ARIAN-Hinshelwood mechanism.<sup>1,2</sup> Layered double hydroxides (LDHs) have a general formula of [M2+1-xM3+x-(OH)<sub>2</sub>]<sup>x+</sup>(A)<sup>n-</sup><sub>x/n</sub>⋅ mH<sub>2</sub>O and consist of highly ordered two-dimensional hydroxide layers where M<sup>2+</sup> and M<sup>3+</sup> are divalent and trivalent cations respectively and A<sup>n-</sup> is the interlayer anion of valence n like carbonate, nitrate and so on,<sup>3-5</sup> Fig. S1(a). LDHs are used in artificial photosynthesis, biomedical sectors, oxygen evolution reaction towards efficient hydrogen generation,8 controlled drug release and delivery9 and as adsorbent,10 corrosion inhibitors,11 supercapacitors12 and inorganic flame-retardant fillers. 13 In this work, Co-Al-LDH was used for adsorption of MnO<sub>4</sub> ions and catalyzed their reduction to MnO<sub>2</sub>. As reported before, Co-Al-LDH was used as catalyst for reduction of dyes,14 CO2 reduction in aqueous media,15 efficient superoxide dismutase-like nanozyme, 16 enhanced catalyst for carbon-carbon coupling<sup>17</sup> and as one of components of a photocatalyst. 18

MoS<sub>2</sub> is a natural or synthetic compound and has a layered structure. In its structure, a plane of molybdenum atoms is sandwiched by two planes of sulfide ions which form a layer. These three planes stack on top of each other with strong covalent bonds between the Mo and S atoms and weak van der Waals forces hold these layers together,<sup>2,19–21</sup> Fig. S1(b). MoS<sub>2</sub> shows polytypism and has three various configurations like 1T,22 2H23 and 3R24 that represent its trigonal, hexagonal and rhombohedral arrangements, respectively and among them 2H is the most stable thermodynamic form of MoS<sub>2</sub>.<sup>23</sup> MoS<sub>2</sub> possesses many applications such as solid lubricant,<sup>25</sup> biosensor,<sup>26</sup> gas sensor,<sup>27</sup> catalyst,<sup>28</sup> supercapacitor<sup>29</sup> and for tissue engineering,<sup>30</sup> electronic and optoelectronic devices,<sup>31</sup> energy storage,<sup>32</sup> solar energy storage,<sup>33</sup> and biomedical applications.34

Potassium permanganate (KMnO<sub>4</sub>), known as "Condy's Crystal", is a strong oxidizing inorganic compound and has many applications like medical uses,<sup>35</sup> water treatment process<sup>36</sup>, analytical uses<sup>37</sup> and synthesis of organic compounds<sup>38</sup> in laboratories and industry.

In this study, as-synthesized carbonate intercalated Co-Al-LDH and MoS2 were used as highly efficient adsorbents for MnO<sub>4</sub>. In our previous works,<sup>1,2</sup> both Co-Al-LDH and MoS<sub>2</sub> were characterized by various techniques such as FTIR (Fourier transfer infrared spectroscopy), BET (Brauner-Emmett-Teller), FESEM (field emission scanning electron micrograph), EDS (energy dispersive X-ray spectroscopy), XPS (X-ray photoelectron spectroscopy) and XRD (X-ray diffraction). Here, we studied effects of different variables like pH, initial MnO<sub>4</sub> concentration, temperature, shaking rate, contact time and ionic strength on adsorption capacity of Co-Al-LDH and MoS2 for MnO<sub>4</sub> . Also, in this work, NIPPON equation was introduced for analysis of adsorption kinetic process. The kinetics of adsorption of MnO<sub>4</sub> on Co-Al-LDH and MoS<sub>2</sub> were analyzed by the KASRA model and the KASRA, Elovich, intraparticle diffusion, ISO and NIPPON equations to give more information about the mechanism of these processes. In this study, using information obtained from carrying out kinetic tests and our previous works, 1,2 mechanism of adsorption kinetics of MnO<sub>4</sub> on Co-Al-LDH and MoS<sub>2</sub> were investigated.

#### 2. Materials and Methods

#### 2. 1. Chemicals

Aluminum nitrate ( $Al(NO_3)_3.9H_2O$ ) (>98.5%), cobalt nitrate ( $Co(NO_3)_2.6H_2O$ ) (>99%), sodium carbonate (99.9%), sodium molybdate ( $Na_2MoO_4.2H_2O$ ) (>99.5%), thioacetamide (>99%), hydrochloric acid (37%), concentrated sulfuric acid (98%), oxalic acid (>99%), sodium hydroxide (>98%), sodium chloride (>99.5%) and potassium permanganate (>99%) were purchased from Merck. All chemicals were used without further purification.

#### 2. 2. Synthesis of Co-Al-LDH and MoS<sub>2</sub>

Synthesis of carbonate intercalated Co-Al-LDH was carried out according to the procedure for preparation of carbonate intercalated Mg-Al-LDH (Mg<sub>6</sub>Al<sub>2</sub>(OH)<sub>16</sub>CO<sub>3</sub> · 4H<sub>2</sub>O)<sup>39</sup> in our previous works.  $^{1,40}$  The MoS<sub>2</sub> was prepared according to the published procedure.  $^{2,41}$ 

## 2. 3. Characteristics of As-synthesized Co-Al-LDH and MoS<sub>2</sub>

The synthesized Co-Al-LDH and MoS<sub>2</sub> were characterized by XRD, SEM, EDS, FTIR, BET and XPS techniques which confirmed their formation<sup>1,2</sup> and were used for studying thermodynamics<sup>1,2</sup> and kinetics of adsorption of MnO<sub>4</sub> on Co-Al-LDH and MoS<sub>2</sub>. It was shown that MnO<sub>4</sub> ions were adsorbed on the mesopore and micropore adsorption sites of Co-Al-LDH and micropore adsorption sites of MoS<sub>2</sub> nanocompounds. Mesopore and micropore adsorption sites were abbreviated as ME and MI sites, respectively.

#### 2. 4. Adsorption Kinetic Tests

In adsorption kinetic tests, 0.002 g of Co-Al-LDH or 0.0015 g of MoS<sub>2</sub> samples were added to 10 ml of MnO<sub>4</sub> solutions. Initial concentrations of MnO<sub>4</sub> solutions were  $2 \times 10^{-5}$ ,  $5 \times 10^{-4}$  or  $7 \times 10^{-4}$  M in the case of Co-Al-LDH and  $2.5 \times 10^{-4}$ ,  $5 \times 10^{-4}$  or  $0.75 \times 10^{-4}$  M for MoS<sub>2</sub>. The solutions were shaken at 40, 70 and 100 rpm in a temperature controlled water bath shaker (Fater electronic Co., Persian Gulf model) at 308, 318 and 328 K and different ionic strengths and pHs. The residual concentrations of MnO<sub>4</sub> in the solutions were measured at different contact times during the course of adsorption, through photometry at their  $\lambda_{max}$  values by a UV mini 1240V Shimadzu spectrophotometer. The  $\lambda_{max}$  values of MnO<sub>4</sub> in neutral water, acidic and alkaline media were 527 and 546 nm and that of MnO $_4^{2-}$  in alkaline media was 437 nm. The relation used to calculate MnO<sub>4</sub>adsorption capacity on the Co-Al-LDH or MoS<sub>2</sub>,  $q_t$  (mg g<sup>-1</sup>), was as follows

$$q_t = \frac{(c_0 - c_t)Mv}{1000 w} \tag{1}$$

where  $q_t$  is adsorption capacity at time t (mg g<sup>-1</sup>),  $c_0$  and  $c_t$  are the initial concentration of adsorbate in each solution and adsorbate concentration at time t (M) respectively, v is the volume of solution (ml), M is the molecular weight of adsorbate (mg mole<sup>-1</sup>) and w is the weight of the used adsorbent (g).

#### 2. 5. Adsorption Model and Isotherms

In our previous works,<sup>1,2</sup> the adsorption thermodynamic isotherms of MnO<sub>4</sub> on the surface of Co-Al-LDH and MoS<sub>2</sub> were analyzed by "<u>adsorption isotherm regional analysis model</u>" that is abbreviated as the ARIAN model

and their adsorption mechanism were explained by analysis of their adsorption isotherm and other experimental evidence. Here, we explained about this model because we used some results of it along with results of adsorption kinetic tests. The ARIAN model was explained in Supplementary material, 42-46 Fig. S2. Briefly, this model is composed from four regions. Region I is related to adsorption of adsorbate on the most active adsorption sites. Region II is the result of interaction of adsorbate with a group of less active adsorption sites. If there are two or more adsorption sites, the sub-regions of region II are denoted by IIA, IIB, etc. Region III appears in the case of formation of aggregates of adsorbates on the surface like micelles and in region IV plateau appears or in some cases reverse desorption is observed. Adsorption kinetic tests of MnO<sub>4</sub> on the Co-Al-LDH and MoS2 were carried out within regions I and II of their isotherms and compared with each other.<sup>1,2</sup>

#### 2. 6. Adsorption Kinetic Equations and Model

The kinetic curves were studied by several equations. The intraparticle diffusion equation<sup>47</sup> is given by

$$q_{I} = k_{dif} t^{0.5} + I (2)$$

where I is the boundary layer thickness and  $k_{dif}$  is the rate constant for intraparticle diffusion.

Another equation used for analysis of adsorption kinetics is the Elovich equation<sup>48</sup> that is written as

$$q_{t} = \frac{1}{\beta} \ln(\alpha \beta) + \frac{1}{\beta} \ln t \tag{3}$$

where  $\alpha$  is initial adsorption rate and  $\beta$  is the Elovich constant.

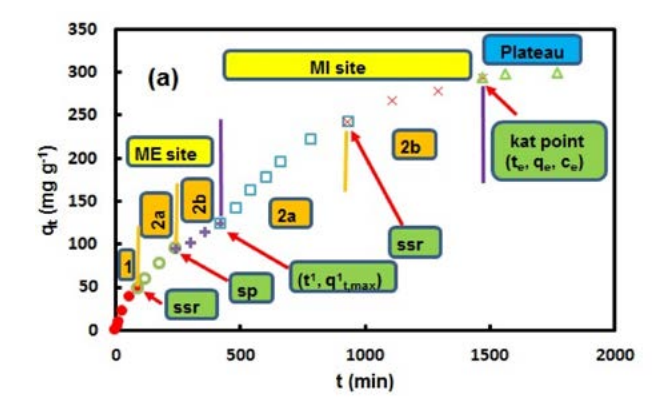
Also, the KASRA model and KASRA equation<sup>49–51</sup> were used to analyze the adsorption kinetics. KASRA is an abbreviation for "kinetics of adsorption study in the regions with constant adsorption acceleration". KASRA is a Persian word meaning king. The KASRA model is based on the three assumptions for adsorption of an adsorbate species on an adsorption site: (1) each time range that adsorption acceleration in it is constant, is named a "region", (2) there are two regions before reaching the plateau region, and (3) the boundary between the first and second regions is called starting second region (abbreviated as ssr) point and that of between the second and third regions is called *start*ing third region (abbreviated as str) point that of between the third and fourth (plateau) regions is called kinetics of adsorption termination (abbreviated as kat) point. All of these points are determined by the KASRA equation<sup>49,50</sup> given as follows:

$$q_{t} = \frac{1}{2}a_{i}t^{2} + (v_{0i} - a_{i}t_{0i})t + q_{0i} - \frac{1}{2}a_{i}t_{0i}^{2} - (v_{0i} - a_{i}t_{0i})t_{0i}$$
 (4)

where  $q_{0i}$ ,  $v_{0i}$  and  $t_{0i}$  are  $q_t$ , velocity and time at the beginning of the *ith* region, respectively and  $a_i$  is the acceleration

of adsorption kinetics in the *ith* region whereas i=1-4. In these works, due to lack of the third region and thus *str* point, the point between the second and fourth regions was called *kat* point and thus i=1-3. Each  $a_i$  is a negative value because during adsorption process the adsorbate concentration decreases. In the first region,  $t_{01}$  and  $q_{01}$  are equal to zero. The second region begins from *ssr* point which is assigned with the coordinates  $t_{02}$  and  $q_{02}$ . Finally, plateau (third) region starts at the equilibrium time,  $t_e$  and equilibrium adsorption capacity,  $q_e$  which are coordinates of *kat* point. In this region,  $v_{03} = a_3 = 0$ ,  $t_{03} = t_e$  and  $q_{03} = q_e$  and Eq. (4) is simplified to  $q_t = q_e$ . Due to different characteristics of the first and second regions, parameters obtained for these two regions such as rate constants are different from each other.

In this work, to avoid confusion in relation to the regions in isotherms and kinetic curves, kinetic regions are shown using numbers like region 1, etc. Typical adsorption kinetic curves of  $MnO_4^-$  on Co-Al-LDH and  $MoS_2$  according to the KASRA model were shown in Fig. 1.



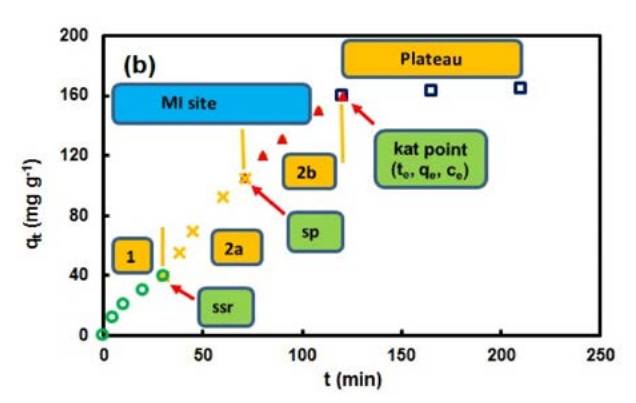


Fig. 1 Typical adsorption kinetic diagrams of MnO $_4^-$  on (a) Co-Al-LDH and (b) MoS $_2$  based on the KASRA model

The  $\underline{i}deal$ - $\underline{s}econd$ - $\underline{o}rder$  (or abbreviated as ISO) equation<sup>50</sup> is written as

$$\ln\left(\frac{q_e - q_t}{ac_t}\right) = -\frac{k_I c_e}{q_e} t + A' \tag{5}$$

where  $k_I = k_I^2 q_e$  and  $k_I^2$  are the first- and second-order adsorption rate constants of the ISO equation in each region

and are in  $M^{-1}$  mg  $g^{-1}$  min<sup>-1</sup> and  $M^{-1}$  min<sup>-1</sup>, respectively and  $M^{-1}$  in  $\left(\frac{q_e}{ac_e}\right)^{-46}$   $a = \frac{Mv}{1000w}$ , where v is the volume of solution (ml), w is the weight of the used adsorbent (g) and M is the molecular weight of adsorbate (mg mole<sup>-1</sup>). A number of adsorbents have m different adsorption sites and adsorption occurs in sequence on their first, then second, ..., (m-1)th and mth sites, respectively. In these cases, there are m kinetic curves and in Eq. (5),  $q_e$  and  $c_e$  are used for mth site and for m-1 other sites and these symbols are replaced with  $q_{t,\max}^i$  and  $c_{t,\max}^i$ , where i=1, ..., m-1.  $q_{t,\max}^i$  and  $c_{t,\max}^i$  are the maximum adsorption capacity of adsorbent and adsorbate concentration after absorption completion on the ith adsorption site, respectively. Thus, the ISO equation is used m times to analyze these m kinetic curves.  $^{46}$ 

As referred before, in this work due to lack of the third region, based on the KASRA model there are two regions in adsorption kinetic curves before reaching the plateau which result from non-ideality in adsorption process. In the first one, completely ideal adsorption occurs on the bare surface of adsorbent. The progressively changes happened on the surface of adsorbent in region 1 finally result in emerging another ideal region (region 2) in which adsorption carries out on a partly adsorbate-covered surface.

But, using the ISO equation shows that region 2 is composed of two another ideal parts that are named 2a and 2b. The first part of the second region, 2a, starts after *ssr* point and the second one, 2b, starts after *starting second part* (or abbreviated as *sp*) point and ends at the *kat* point.<sup>49</sup>

The ISO first-order rate constant of region 1 is shown with  $k_{I1}$  and those of the second region are shown with  $k_{I2a}$  and  $k_{I2a}$ , respectively. Also, the ISO second-order rate constant of region 1 is shown with  $k_{I1}^2$  and those of the second region are shown with  $k_{I2a}^2$  and  $k_{I2b}^2$ , respectively. Due to decrease in adsorbate concentration with time, the ISO rate constant of region 1 is greater than part a of region 2 or part 2a, i.e.  $k_{I1} > k_{I2a}$  and in part b of region 2 (or part 2b), adsorption ends to plateau and due to this sudden change  $k_{I2b}$  is greater than both  $k_{I1}$  and  $k_{I2a}$ , thus we have  $k_{I2b} > k_{I1} > k_{I2a}$ . Similarly, for the ISO second-order rate constants we have  $k_{I2b}^2 > k_{I1}^2 > k_{I2a}^2$ .

If the ISO rate constant of a step obeys the Arrhenius equation, that step is adsorption- or reaction-controlled and otherwise it is called diffusion-controlled. As referred above, in some adsorbents, there are two or more different adsorption sites which result in observing two or more successive adsorption kinetic curves in an adsorption kinetic diagram. In these cases, region 1, (completely ideal) is only observed in the first adsorption kinetic curve, <sup>46</sup> Fig. 1.

Sometimes, due to braking effect<sup>50</sup> an interval is observed between two successive adsorption kinetic curves or between regions 1 and 2 of the first adsorption curve. The "time range of interval between two successive adsorption kinetic curves" (abbreviated as TRAK) is used to compare this effect in different cases.<sup>46,51</sup> On the other hand, the initial concentration of adsorbate has an important role in

appearing the TRAK in an adsorption kinetic curve. Thus, for comparing kinetic curves including TRAK(s) with together and other kinetic curves, their first-order rate constants obtained from the ISO equation are used.

If adsorption results in a TRAK,  $q_{t,\max}^i$  and  $c_{t,\max}^i$  are replaced by  $c_T^q$  and  $c_T^n$ , respectively.  $q_T^n$  and  $c_T^n$  are adsorption capacity of adsorbent and adsorbate concentration at the beginning of the TRAK between nth and (n+1)th kinetic curves, respectively. In these cases,  $k_i = k_L^2$ ,  $q_T^n$  and subscript T is an abbreviation for TRAK.  $^{46,51}$ 

#### 2. 7. Introducing the NIPPON Equation

Adsorption on heterogeneous surface of adsorbents in liquid phase happens through different kinds of interactions, like hydrogen bonding, between adsorbate species and some parts (and not whole) of adsorbents surface. Also, at first, most active sites and then other less active sites of adsorbent surface interact with adsorbate species. Thus, adsorption thermodynamics and kinetics in liquid phase are intrinsically non-ideal. As explained in the KASRA model and ISO equation, adsorption on the most active and less active adsorption sites of the same type or adsorption on different types of adsorption sites on an adsorbent are separately studied as ideal cases and have different adsorption kinetic parameters. 46,49,50 In the KASRA model, adsorption capacity was written as a threeterm polynomial function of time. But, as in physics higher derivatives of position with respect to time are used for non-ideal situation,<sup>52,53</sup> we can use higher derivatives of adsorption capacities with respect to time to analyze the non-ideal adsorption kinetic data to find average parameters of the same type adsorption sites that have different activities. By considering a time range of adsorption kinetics belonging to one average type of adsorption site as a continuous non-ideal process, the time function of non-ideal adsorption capacity,  $q_t$  changes with time as  $\hat{\Sigma}^{(-1)^{n}t^{n}}$  which is the Taylor series of  $\frac{1}{1+l}$ . Here, N is an abbreviation for "non-ideal adsorption". In spite of the KASRA equation, in non-ideal adsorption it was assumed that in each time range adsorbate species were simultaneously adsorbed on adsorption sites with different activities. Thus, changes in  $q_t$  with time was written as

$$\frac{dq_t^N}{dt} = k(1 - t + t^2 - t^3 + t^4 - \dots)$$
 (6)

By using the relation  $\frac{1}{1+t} = 1 - t + t^2 - t^3 + t^4 \dots$ , Eq. (6) can be written as

$$\frac{dq_i^N}{dt} = k \left(\frac{1}{1+t}\right) \tag{7}$$

where *k* is the rate constant of the equation (6). By integration of Eq. (7) we have

$$\int dq_t^N = k \int \frac{dt}{1+t} \tag{8}$$

$$q_t^N = k \ln(1+t) + cte \tag{9}$$

where  $cte = q_{ts}^N + k \ln(1 + t_s)$ .  $q_{ts}^N$  and  $t_s$  are adsorption capacity and time in the starting point of the assumed time range, respectively. When t << 1 we have  $\ln(1 + t) \approx t$  and then

$$q_t^N = kt$$
 (10)

Dimension of natural logarithm argument, 1 + t, is in  $\frac{time}{1 \text{ unit of time}}$ . Equation (9) was derived and introduced by one of authors, Babak Samiey, and was called " $\underline{non-ideal}$   $\underline{process}$  of  $\underline{adsorption}$   $\underline{kinetics}$   $\underline{equation}$ " or abbreviated as the NIPPON equation, Fig. 2.

NIPPON is a Japanese name of Japan and means the sun's origin. By taking the first and second derivatives of the NIPPON equation, non-ideal velocity and non-ideal acceleration adsorption kinetic equations, Eqs. (11) and (12), were obtained respectively. These equations are as follows

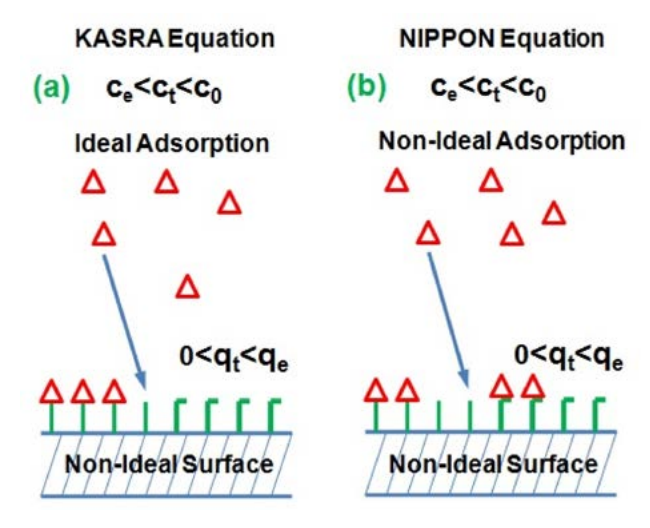


**Fig. 2** Schematic comparison of adsorption kinetics by the (a) KAS-RA and (b) NIPPON equations. One type of functional group as adsorption site with two different types of activities was shown in green and adsorbate species were shown in red

**Table 1.** Adsorption acceleration and velocity parameters for the first and second region and related  $t_{ssr}$  and  $q_{ssr}$  values obtained from analysis of some adsorption processes by the KASRA model

Sym-	Adsorption process	First	region			Secor	nd region	
bol		$a_{01}$	$v_{01}$	$t_{ssr}$	$q_{ssr}$	$a_{02}$	$v_{02}$	Ref.
A	Adsorption of oxalic acid on animal charcoal at 308 K	0	$9.0 \times 10^{-3}$	10	0.02	$-2.0 \times 10^{-5}$	$2.0 \times 10^{-2}$	54
В	Adsorption of natural dissolved organic matter (in terms	0	0.33	5.3	1.4	$-6.7 \times 10^{-5}$	$8.7 \times 10^{-3}$	55
	of DOC) by multiwalled carbon nanotubes at 5 °C							
C	Adsorption of natural dissolved organic matter (in	$2.0 \times 10$	$^{-4}$ 5.2 × 10 <sup>-3</sup>	20.3	0.08	$-1.2 \times 10^{-5}$	$9.2 \times 10^{-4}$	55
	terms of AOC) by multiwalled carbon nanotubes at 5 °C							
D	Adsorption of direct yellow12 on coconut shell activated carbon	-0.02	1.46	10	14.9	$-1.4 \times 10^{-4}$	1.49	56
E	Adsorption of basic blue 3 onto sphagnum agellanicum pe	eat 0	9.75	1.2	11.7	$-3.6 \times 10^{-2}$	0.54	57
F	Adsorption of reactive red 239 from aqueous solution	-0.17	0.61	10	9.6	$-4.0 \times 10^{-3}$	0.24	58
-	by chitosan 8B	0.17	0.01	10	,,,	1.0 // 10	V. <b>2</b> 1	-
G	Adsorption of methylene blue on activated carbon	0	13.90	10.3	143.4	$-3.8 \times 10^{-2}$	2.88	59
	obtained from waste Elaeagnus stone	-						
Н	Adsorption of malachite green on activated carbon	0	20.90	9.6	200.7	$-5.6 \times 10^{-2}$	4.75	59
	obtained from waste Elaeagnus stone	-					, -	
I	Adsorption of rhodamine B on activated carbon obtained	0	14.27	10.3	147.0	$-2.4 \times 10^{-2}$	2.30	59
	from waste Elaeagnus stone							
J	Adsorption of methyl orange on banana peel*	0	0.16	5	0.8	$-4.0 \times 10^{-3}$	0.27	60
K	Adsorption of methylene blue on orange peel*	0	0.30	5	1.5	-0.01	0.45	60
L	Adsorption of methylene blue on poly(acrylic acid)	0	5.72	12.8	73.2	$-8.4 \times 10^{-2}$	10.45	61
	(PAA)-based super-adsorbent nanocomposite hydrogel							
M	Adsorption of remazol Y onto steam-activated carbons	0	24.52	1.7	41.7	-0.12	2.03	62
	developed from date pits at pH = 3 and 37 °C							
N	Adsorption of methylene blue onto steam-activated	0	88.58	1.2	106.3	$-8.8 \times 10^{-2}$	2.95	62
	carbons developed from date pits at pH = 5 and 27 $^{\circ}$ C							
O	Adsorption of acid red on corn stalks modified	0	2.03	3.5	7.1	$-4.0 \times 10^{-3}$	0.26	63
	bycetylpyridinium bromide at 328 K							
P	Adsorption of acid orange on corn stalks modified	0	2.28	5.6	10.5	$-2.0 \times 10^{-3}$	0.15	63
	bycetylpyridinium bromide at 318 K							
Q	Adsorption of malachite green on seeds of dates at 15 °C	-0.60	6.75	14.2	92.5	-0.39	12.64	64
R	Adsorption of methylene blue on nanocrystalline cellulose	e –4.4 ×	$10^{-2} \ 0.21$	10	2.8	$-8.7 \times 10^{-4}$	0.08	50
	at 318 K and 80 rpm and 0.045 mM methylene blue							

Units of  $a_{01}$  and  $a_{02}$  were in mg g<sup>-1</sup> hour<sup>-2</sup>,  $v_{01}$  and  $v_{02}$  were in mg g<sup>-1</sup> hour<sup>-1</sup> and  $t_{ssr}$  and  $q_{ssr}$  were in hour and mg g<sup>-1</sup> in example L and  $a_{01}$  and  $a_{02}$  were in  $\mu$ mol g<sup>-1</sup> min<sup>-2</sup>,  $v_{01}$  and  $v_{02}$  were in  $\mu$ mol g<sup>-1</sup> min<sup>-1</sup> and  $t_{ssr}$  and  $q_{ssr}$  were in min and  $\mu$ mol g<sup>-1</sup> in example F, respectively. In other cases,  $a_{01}$  and  $a_{02}$  were in mg g<sup>-1</sup> min<sup>-2</sup>,  $v_{01}$  and  $v_{02}$  were in mg g<sup>-1</sup> min<sup>-1</sup> and  $t_{ssr}$  and  $q_{ssr}$  were in min and mg g<sup>-1</sup>, respectively. \*In examples J and K, TD values were 2.5 and 2 min before starting adsorption process, respectively.

**Table 2.** Non-ideal adsorption acceleration and velocity parameters for the first and second NIPPON curves and related  $t_{sc}$  and  $q_{sc}^N$  values obtained from analysis of some adsorption processes by the NIPPON and KASRA equations

Sym-	Adsorption process	First	curve			Secor	nd curve	
bol	• •	$a_{fc}^N$	$oldsymbol{v_{fc}^N}$	$t_{sc}$	$q_{sc}^N$	$a_{sc}^N$	$v_{sc}^N$	Ref.
A	Adsorption of oxalic acid on animal charcoal at 308 K	-0.01	0.01	_	_	_	_	54
В	Adsorption of natural dissolved organic matter (in terms of DOC) by multiwalled carbon nanotubes at 5 $^{\circ}$ C	0	0.33	5.3	1.4	-0.005	0.03	55
С	Adsorption of natural dissolved organic matter (in terms of AOC) by multiwalled carbon nanotubes at 5 °C	0.035	-0.035	_	_	-	_	55
D	Adsorption of direct yellow12 on coconut shell activated carbon	0	1.49	20	30.2	-0.46	5.02	56
E	Adsorption of basic blue 3 onto sphagnum agellanicum p	eat 0	9.75	1.2	11.7	-0.59	1.29	57
F	Adsorption of reactive red 239 from aqueous solution by chitosan 8B	-4.18	4.18	-	-	-	-	58
G	Adsorption of methylene blue on activated carbon obtained from waste Elaeagnus stone	-17.88	17.88	_	_	-	_	59
Н	Adsorption of malachite green on activated carbon obtained from waste Elaeagnus stone	-19.07	19.07	_	_	-	_	59
I	Adsorption of rhodamine B on activated carbon obtained from waste Elaeagnus stone	-17.54	17.54	_	_	-	-	59
J	Adsorption of methyl orange on banana peel*	0	0.16	5	0.8	-0.10	0.61	60
K	Adsorption of methylene blue on orange peel*	0	0.30	5	1.5	-0.15	0.88	60
L	Adsorption of methylene blue on poly(acrylic acid) (PAA)-based super-adsorbent a nocomposite hydrogel	0	5.72	12.8	73.2	-1.51	20.79	61
M	Adsorption of remazol Y onto steam-activated carbons developedfrom date pits at pH=3 and 37 °C	0	24.52	1.7	41.7	-1.47	3.96	62
N	Adsorption of methylene blue onto steam-activated carbons developed from date pits at pH=5 and 27 °C	0	88.58	1.2	106.3	-5.15	11.32	62
O	Adsorption of acid red on corn stalks modified by cetylpyridinium bromide at 328 K	0	2.03	3.5	7.1	-0.14	0.63	63
P	Adsorption of acid orange on corn stalks modified by cetylpyridinium bromide at 318 K	0	2.28	5.6	10.5	-0.05	0.31	63
Q	Adsorption of malachite green on seeds of dates at 15 °C	-56.61	56.61	_	_	_	_	64
R	Adsorption of methylene blue on nanocrystalline cellulose at 318 K and 80 rpm and 0.045 mM methylene b	-1.34 blue	1.34	-	_	-	-	50

Units of  $a_{sc}^N$  and  $a_{sc}^N$  were in mg g<sup>-1</sup> hour<sup>-2</sup>,  $v_{sc}^N$  and  $v_{sc}^N$  were in mg g<sup>-1</sup> hour<sup>-1</sup> and  $t_{sc}$  and  $q_{sc}^N$  were in hour and mg g<sup>-1</sup> in example L and  $a_{sc}^N$  and  $a_{sc}^N$  were in  $\mu$ mol g<sup>-1</sup> min<sup>-2</sup>,  $v_{sc}^N$  and  $v_{sc}^N$  were in  $\mu$ mol g<sup>-1</sup> min<sup>-1</sup> and  $t_{sc}$  and  $q_{sc}^N$  were in min and  $\mu$ mol g<sup>-1</sup> in example F, respectively. In other cases,  $a_{sc}^N$  and  $a_{sc}^N$  were in mg g<sup>-1</sup> min<sup>-2</sup>,  $v_{sc}^N$  and  $v_{sc}^N$  were in mg g<sup>-1</sup> min<sup>-1</sup> and  $t_{sc}$  and  $q_{sc}^N$  were in min and mg g<sup>-1</sup>, respectively. \*In examples J and K, TD values were 2.5 and 2 min, and thus for first curve, and min were used in Eqs. (11) and (12), respectively. Subscripts fc and sc are abbreviations for starting first curve and starting second curve, respectively.

$$v_t^N = \frac{k}{1+t} \tag{11}$$

$$a_{t}^{N} = -\frac{k}{(1+t)^{2}} \tag{12}$$

where  $v_t^N$  and  $a_t^N$  were non-ideal velocity and acceleration of adsorption of adsorbate, respectively. On the other hand, at t = 0,  $v_0^N = k$  and  $a_0^N = -k$  and  $t = t_e$  we have

$$v_e^N = \lim_{t \to \infty} \frac{k}{1+t} = 0 \tag{13}$$

$$a_e^N = -\lim \frac{k}{(1+t)^2} = 0 \tag{14}$$

where  $v_e^N$  and  $a_e^N$  were non-ideal velocity and acceleration of adsorption of adsorbate at  $t = t_e$ , respectively. In initial time ranges of adsorption, the process is ideal and may obey from the KASRA equation.

In some adsorption processes, depending on the nature of adsorbent or adsorbate, it is possible to observe more than one curve. A number of examples chosen from published papers<sup>50,54–64</sup> were analyzed by the KASRA model, Table 1 and Fig. S3 and the NIPPON equation, Table 2 and Fig. S4. Here, to calculate non-ideal velocity and acceleration of adsorption of adsorbates by using equations (11) and (12), and were used for the first and second curves, respectively.

#### 3. Results and Discussion

## 3. 1. Characterization of Co-Al-LDH and MoS<sub>2</sub> Nanocompounds

Characterization of these two compounds by XRD, XPS, FTIR, SEM, BET and EDS techniques showed that in this work  $Co_6Al_2(OH)_{16}CO_3.4H_2O$  and hexagonal

 $2H\text{-MoS}_2$  were synthesized.<sup>1,2</sup> Analysis of products of adsorption of MnO $_4$  on Co-Al-LDH verified that Co-Al-LDH catalyzed reduction of MnO $_4$ ions to MnO $_2$  in the pH range of 1–13 and reacted with it at pH=14. Study of data showed that its adsorption sites are Co–OH groups located on ME and MI sites.<sup>1</sup>

On the other hand, analysis of products of MnO<sub>4</sub> adsorption on MoS<sub>2</sub> confirmed that MnO<sub>4</sub> reacted with MoS<sub>2</sub> in the pH range of 1–12 and its adsorption sites were Mo–S pairs located on its micropore sites.<sup>2</sup>

### 3. 2. Kinetics of adsorption of MnO<sub>4</sub> on Co-Al-LDH

As reported before, <sup>65–69</sup> Co-Al-LDH was used as an adsorbent or one of components of an adsorbent and kinetics and thermodynamics of these processes were studied by researchers. As observed in our earlier work, <sup>1</sup> the boundary of regions of adsorption isotherms of MnO<sub>4</sub> on Co-Al-LDH under different conditions were shown in Table S1. Based on these data, appropriate initial concentrations of MnO<sub>4</sub> were used for doing adsorption kinetic tests.

The adsorption kinetics of  $MnO_4^-$  on Co-Al-LDH was studied using various initial  $MnO_4^-$  concentrations of 0.25, 0.5 and 0.7 mM, shaking rates of 40, 70 and 100 rpm at 308, 318 and 328 K in water (neutral water), 0.1 M NaCl and in acidic (pHs of 2.8, 3.8) and alkaline (pHs of 12, 13 and 14) solutions, shown in Tables 3–7 and Figs. 3, 4 and S5. Under different conditions,  $MnO_4^-$  ions were adsorbed on the surface of Co-Al-LDH after 10 h.

As seen in Tables 4 and 6, in water, at 100 rpm and in 0.25 mM  $\mathrm{MnO_4^-}$  (in region I of the thermodynamic AR-IAN model)  $\mathrm{MnO_4^-}$  ions were adsorbed on ME adsorption sites. However, in initial  $\mathrm{MnO_4^-}$  concentrations of 0.5 and 0.7 mM (in region II of the thermodynamic ARIAN model) in water and 0.1 M NaCl,  $\mathrm{MnO_4^-}$  ions were adsorbed on both ME and MI adsorption sites. Tests showed that an increase in the initial  $\mathrm{MnO_4^-}$  concentration, shaking rate, temperature or ionic strength (other parameters were constant) increased the values of  $k_{dif}$ , adsorption acceleration, initial adsorption rates,  $k_{I1}$  and  $k_{I2b}$  (both for kinetic curve of adsorption on ME sites), and  $k_{I2a}$  (for kinetic curve of adsorption on ME sites was composed of only one part and its value was greater than that of region 1 thus it was part 2b.

In 0.1 M NaCl solution, an increase in  $k_{dif}$ , adsorption acceleration, initial adsorption rates and a vigorous increase in  $k_{I1}$  and  $k_{I2b}$  (both for adsorption on ME sites) and  $k_{I2a}$  (for adsorption on MI sites) was observed compared to those in water at 318 K was due to that  $CO_3^2$ —ions were surrounded by Na<sup>+</sup> ions, which decreased electric repulsion between  $CO_4^2$ —and MnO $_4$ -ions. Also, an initial high adsorption capacity for MnO $_4$ —ions resulted in emerging a TRAK in its adsorption kinetic curve, Table 3. Activation energies of  $k_{I1}$  and  $k_{I2b}$  (both for the adsorption on

ME sites) and  $k_{12a}$  (for the adsorption on MI sites) in water were 60.4, 75.1 and 49.1 kJ mole<sup>-1</sup>, respectively which showed that these steps were adsorption-controlled.

In acidic solutions, adsorption process happened only on ME adsorption sites which was due to the formation of bigger neutral  $\mathrm{HMnO_4}$  molecules. <sup>70</sup> Because of a decrease in formal charge of  $\mathrm{MnO_4^-}$  ions,  $k_{dif}$  adsorption acceleration, initial adsorption rates,  $k_{I1}$  and  $k_{I2b}$  decreased with a decrease in pH of solutions from 3.8 to 2.8.

In acidic solutions, due to the increase in ionic strength and the acidity of solution that promoted adsorption capacity, we noticed that  $k_{dif}$  adsorption acceleration, initial adsorption rates,  $k_{I1}$  and  $k_{I2b}$  values increased compared with those in water at 318 K.

In alkaline environment, it was observed that with an increase in pH value to 12,  $k_{dif}$ , adsorption acceleration, initial adsorption rates,  $k_{I1}$  and  $k_{I2b}$  (both on ME adsorption sites) highly increased due to an increase in the number of –OH groups of adsorbent surface and ionic strength of the solution. pH<sub>ZPC</sub> (pH of zero point charge) of carbonate intercalated Co-Al-LDH is 10 and in pHs of higher than 10 its surface charge is negative and became more negative with an increase in pH value.<sup>71</sup> Thus, further increase in pH to 13 yielded in a decrease in  $k_{dif}$ , adsorption acceleration, initial adsorption rates,  $k_{I1}$  and  $k_{I2b}$  because of the neutralization of amphoteric Al–OH groups of adsorbent, and also changing large amount of MnO $_4^2$  Tables 4 and 5.

At pH=13, due to neutralization of some hydroxide groups and increasing adsorbent surface negative charge, MnO $_4^-$  ions were adsorbed only on ME sites. Activation energies of  $k_{I1}$  (for adsorption on ME sites) was 46.3 kJ mole $^{-1}$  which showed that the kinetics of this step was adsorption-controlled, similar to that in water. However,  $k_{I2b}$  values did not obey Arrhenius equation that confirmed that kinetics of adsorption of MnO $_4^-$  ions in this step was diffusion-controlled.

At pH=14, similar to pH of 13,  $MnO_4^-$  ions were adsorbed on ME sites and due to very fast adsorption and reaction of  $MnO_4^-$  ions with ME adsorption sites,  $q_t$  value of ME sites reached 112.2 mg g<sup>-1</sup> (about 50% of total adsorption capacity of adsorbent) within less than half minute after the adsorption test started.

Because of the consumption of  $MnO_4^-$  ions, a TRAK was observed in the range of less than 0.5 min to 180 min, Table 3. After about 2 hours, a gradual production of  $MnO_4^-$  ions from  $MnO_4^{2^-}$  ions in solution resulted in the continuation of adsorption process, Tables 3 and 4. Comparison of EDS spectra of adsorbent samples after 1.5 and 8 hours in 1 mM  $MnO_4^-$  solutions at pH of 14 showed that about 75% of manganese adsorption occurred after 1.5 h contact with adsorbate solution, Fig. S6.

Analysis of adsorption kinetic data of  $MnO_4^-$  on Co-Al-LDH by NIPPON equation showed that an excess ideal curve was observed in the beginning of adsorption kinetic diagrams of 2.5 mM  $MnO_4^-$  at 318 K, 0.5 mM  $MnO_4^-$  at 328 K, 0.7 mM  $MnO_4^-$  at 318 K in water and in 0.5 mM

MnO<sub>4</sub> at pHs of 2.8, 3.8, 12 at 328 K and at pH of 13 at 308, 318 and 328 K at 100 rpm compared to analysis with the KASRA model. These observations showed that activities of the most active adsorption sites located in initial time ranges of first region obtained from the KASRA model were somehow bigger than activities of rest of this type of adsorption sites.

Analysis of adsorption kinetic diagrams of 0.5 mM MnO<sub>4</sub> at 308 and 318 K at 100 rpm and 0.5 mM MnO<sub>4</sub> at 318 K at 70 rpm by NIPPON equation showed that there were no excess ideal curve in the beginning of them compared to regions obtained from the KASRA model. In cases 0.5 mM MnO<sub>4</sub> at 308 and 318 K at 100 rpm, second curves were bigger than those obtained from the KASRA model that showed that activities of boundary adsorption sites were more similar to those located in the second region obtained from the KASRA model. In the case of 0.5 mM MnO<sub>4</sub> at 318 K at 70 rpm, it was observed that first curve obtained by NIPPON equation was bigger than that calculated by the KASRA model that showed that the activities of boundary adsorption sites were more similar to those of the first region obtained from the KASRA model.

Because MnO<sub>4</sub> was adsorbed at first on ME sites of Co-Al-LDH, only adsorption of MnO<sub>4</sub> on these sites were studied by the Elovich equation. As shown in Table 7,  $\alpha$ 

values in water increased with an increase in temperature and shaking rate.

On the other hand, as reported before,<sup>1</sup> the used Co-Al-LDH adsorbent was recycled successfully by NaBH<sub>4</sub>.

#### 3. 3. Kinetics of adsorption of MnO<sub>4</sub> on MoS<sub>2</sub>

During recent years, researchers used  $MoS_2$  and its composites as efficient adsorbents. As reported in our previous work, the regions of adsorption isotherms of  $MnO_4^-$  on  $MoS_2$  and their boundaries under different conditions were analyzed by the ARIAN model and were shown in Table S2. Using data of this Table, the appropriate initial concentrations of  $MnO_4^-$  were determined for carrying out adsorption kinetic tests.

The adsorption kinetic curves of  $MnO_4^-$  on  $MoS_2$  were obtained using different initial  $MnO_4^-$  concentrations of 0.25, 0.5 and 0.75 mM, shaking rates of 40, 70 and 100 rpm, at 308, 318 and 328 K in water (neutral water), 0.1 M NaCl and in acidic and alkaline solutions at 318 K, Tables 8–11 and Figs. 5, 6 and S7. Under various conditions,  $MnO_4^-$  ions were adsorbed on the surface of  $MoS_2$  during different time periods (20–180 min) and then reacted with it. Analysis of adsorption kinetics of this process by the KASRA model showed that  $MnO_4^-$  ions were adsorbed on

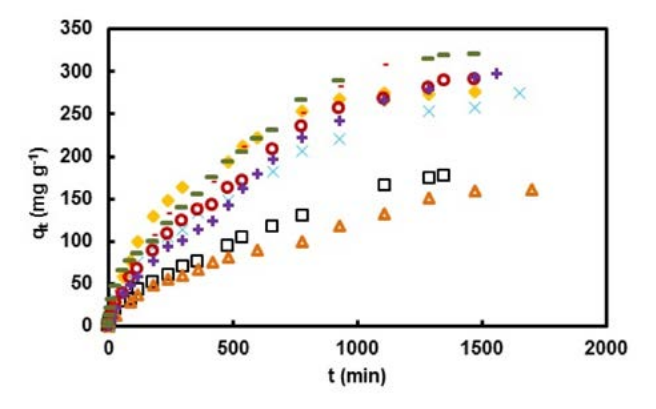
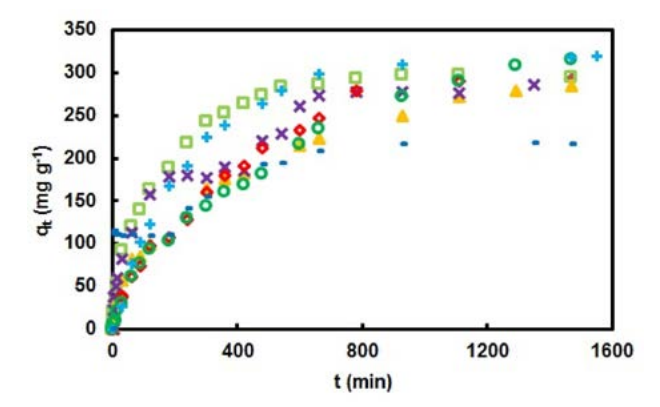


Fig. 3 Kinetic curves of adsorption of MnO $_4^-$  on Co-Al-LDH in water in initial MnO $_4^-$ concentrations of  $_2$  0.25 mM  $_2$  at 318 K, 0.5 mM at  $_3$  308 K,  $_4$  318 K and  $_4$  328 K and  $_4$  0.7 mM at 318 K and  $_4$  0.5 mM in 0.1 M NaCl at 318 K and 100 rpm and also tests were carried out in [MnO $_4^-$ ] $_0$ = 0.5 mM in water and 318 K at + 40 rpm and 0 70 rpm



**Fig. 4** Kinetic curves of adsorption of MnO $_4$  on Co-Al-LDH in pHs of  $\blacktriangle$  2.8,  $\sqcap$  3.8,  $\times$  12 and  $\neg$ 14 at 318 K and pH of 13 at  $\lozenge$  308 K,  $\circ$  318 K and + 328 K at 100 rpm and [MnO $_4$ ] $_0$  = 0.5 mM

Table 3. TRAKs for adsorption of  $\rm MnO_4^-$  on Co-Al-LDH in 0.1 M NaCl and acidic and alkaline solutions at 308–328 K

Solvent	<i>T</i> (K)	[MnO <sub>4</sub> ] <sub>0</sub> (mM)	rpm	$TRAK_{C_1-C_2}$ (min-min)	$q_{TRAK_{C1-C2}} $ $(mg g^{-1})$	t <sub>e</sub> (min)	$q_e \ ({ m mg~g^{-1}})$
0.1 M NaCl*	318	0.5	100	300-360	141.4-141.7	1290	316.3
pH=2.8**	318	0.5	100	60-90	82.5-85.7	1290	278.3
pH=12*	318	0.5	100	180-420	178.3-185.4	660	273.6
pH=14**	318	0.5	100	> 0.5-180	112.2-110.1	930	216.6

 $TRAK_{C_1-C_2}$  is the observed TRAKs between the first and second kinetic curves. \*TRAK appeared at the end of ME sites range. \*\*TRAK was in the time range of ME sites.  $t_e$  is the time of reaching equilibrium.

**Table 4.** Experimental  $t_e, q_e, t_0, q_0, t_0, q_{0,2}, t_0$  and  $q_{0,3}$  values and coefficients obtained from the KASRA equation and  $k_{dif}$  values of intraparticle diffusion equation for kinetics of MnO<sub>4</sub> adsorption on Co-Al-LDH at different temperatures and in various shaking rates and initial  $\mathrm{MnO}_{2}$  concentrations

Sol	Solvent	$\mathbf{L}$	$[\mathrm{MnO_4^-}]_0$	rpm	$(t_e, q_e)$	KASRA region 1 (1st curve)	ion 1 (1s	t curve)	KASF	KASRA region 2 (1st curve)	1st curve)		KASRA	KASRA region 2 (2nd curve)	(2nd cu	rve)
	_	医	(mM)			$a_1$	$v_{01}$	$k_{dif}$	$(t_{02}, q_{02})$	$a_2$	$v_{02}$	$k_{dif}$	$(t_{03}, q_{03})$	$a_3$	$v_{03}$	$k_{dif}$
Col	orresponding to	ing to:				ARIAN region I	on I (ME	(ME Site)	ARIAN	ARIAN section IIA (ME Site	(ME Site)		ARIAN SC	ARIAN section IIB (MI Site)	(MI Sit	( c
Water		318	0.25	100	(1350,177.7)	$-2.0 \times 10^{-2}$	1.00	4.7	(30,20.9)	-9.9×10 <sup>-5</sup>	0.18	5.2		ı	1	1
	~,	308	0.50	100	(1470,160.0)	$-1.3 \times 10^{-3}$	0.39	4.1	(300,59.7)	$-1.9 \times 10^{-4}$	0.13	3.8	(780,100.3)	$-8.5 \times 10^{-5}$	0.18	5.8
		318	0.50	100	(1650,275.6)	$-2.3\times10^{-2}$	1.42	8.9	(60,43.7)	$-2.1\times10^{-3}$	0.54	7.4	(300,113.2)	$-1.4 \times 10^{-4}$	0.25	8.9
		328	0.50	100	(1110,266.7)	$-4.2 \times 10^{-2}$	1.58	8.9	(30,27.3)	$-3.6\times10^{-3}$	0.95	12.3	(240,148.0)	$-2.3\times10^{-4}$	0.31	2.6
		318	0.70	100	(1350,319.3)	$-6.8 \times 10^{-2}$	2.55	8.5	(30,46.3)	$-3.2\times10^{-3}$	0.59	8.7	(180,99.5)	$-2.9 \times 10^{-4}$	0.36	10.2
	3	$318^{A}$	0.50	20	(1290,281.1)	$-1.6 \times 10^{-2}$	1.15	5.9	(60,38.6)	$-1.0 \times 10^{-3}$	0.50	8.2	(420,142.6)	$-3.6\times10^{-4}$	0.31	10.3
_	3	$318^{B}$	0.50	40	(1470,293.7)	$-4.2 \times 10^{-3}$	0.82	6.9	(120,58.7)	$-6.1 \times 10^{-4}$	0.30	6.7	(420,123.8)	$-2.9 \times 10^{-4}$	0.30	11.2
0.11	.1M NaCl	318	0.50	100	(1290,316.3)	-0.46	4.76	10.2	(10,25.0)	$-1.7 \times 10^{-3}$	0.65	6.7	C(360,141.7)	$-3.1 \times 10^{-4}$	0.33	11.3
.Hd		318	0.50	100	(1290,278.3)	$-2.9\times10^{-2}$	2.24	10.8	D(90,85.7)	$-2.0 \times 10^{-4}$	0.29	7.3	ı	ı	ı	ı
pH:		318	0.50	100	(780,293.3)	$-6.8 \times 10^{-2}$	4.03	18.3	(60,120.4)	$-9.3\times10^{-4}$	0.55	11.2	ı	ı	ı	1
pH:		318	0.50	100	(660,273.6)	-0.19	5.53	14.1	(30,82.6)	$-8.2\times10^{-3}$	1.21	11.6	E(420,185.4)	$-8.1 \times 10^{-4}$	0.46	16.8
pH:	pH=13	308	0.50	100	(1110,289.4)	$-6.3\times10^{-3}$	1.14	9.1	(180,107.2)	$-4.8 \times 10^{-4}$	0.42	11.6	ı	ı	ı	ı
pH:		318	0.50	100	(1470,315.7)	$-6.6 \times 10^{-3}$	1.16	9.4	(180,103.8)	$-2.2\times10^{-4}$	0.30	8.8	ı	ı	ı	ı
pH:		328	0.50	100	(930,309.5)	$-8.2 \times 10^{-3}$	1.51	17.4	(120,122.7)	$-1.0 \times 10^{-3}$	0.58	12.1	I	I	ı	ı
pH:		318	0.50	100	(930,216.6)	Very fa	Very fast (0.5 min		(180,110.1)	$-4.8 \times 10^{-4}$	0.31	7.7	ı	ı	ı	ı

Units of  $a_1$ ,  $a_2$  and  $a_3$  are in mg  $g^{-1}$  min<sup>-2</sup> and those of  $v_{01}$ ,  $v_{02}$  and  $v_{03}$  are in mg  $g^{-1}$  min<sup>-1</sup>. Units of  $t_e$ ,  $t_{02}$  and  $t_{03}$  are in min  $g^{-1}$  min  $t_{03}$  are in mg  $g^{-1}$  min  $t_{03}$  and  $t_{03}$  are in mg  $g^{-1}$  min  $t_{03}$  and  $t_{03}$  are in mg  $g^{-1}$  min before starting adsorption process, respectively, C, D, E and F refer to TRAKs in the range of 300–360, 60–90, 180–420 and >0.5–180 min, respectively

**Table 5.** Coefficients of region 1 and region 2 (parts 2a and 2b) of the ISO equation for kinetics of MnO<sub>4</sub> adsorption on different sites of Co-Al-LDH at 308–328 K

Solvent	T (K)	$[\mathrm{MnO}_4^-]_0$ rpm $(\mathrm{mM})$	rpm	$k_{\Pi}$	$(t_{ssr},q_{ssr}) \ ( ext{min,mg g}^{-1})$	$k_{12a}$	$(t_{sp,}q_{sp}) \ (\mathrm{min,mgg^{-1}})$	$k_{12b}$	$[\mathrm{MnO}^4]^I_{t,max}, \ t^I, \ q^I_{t,max}) \ (\mathrm{mM,min,mg\ g}^{-1})$	$k_{I2a}$	$(t_{sp},q_{sp}) \ ( ext{min,mg g}^{-1})$	$k_{12b}$	$([{ m MnO}^4]_e, t_e, q_e)$ (mMmin,mg g <sup>-1</sup> )
	Co	Corresponding to:	g to:		ARIAN r	egion I a	ARIAN region I and section IIA (ME Site)	(ME Site)			ARIAN section IIB (MI Site)	ion IIB	(MI Site)
Water	318	0.25	100	3562	(30,20.9)	130	(360,76.7)	2803	(0.025, 1350, 177.7)	I	1	ı	1
	308	0.50	100	645	(300,59.7)	ı	ı	1075	(0.37, 780, 100.3)	1022	(1290,151.1)	3227	(0.30,1470,160.0)
	318	0.50	100	1841	(90,43.7)	ı	ı	3745	(0.36,300,113.2)	1743	(930,220.4)	3155	(0.15, 1650, 275.6)
	328	0.50	100	2699	(90,27.3)	ı	ı	6391	(0.31,240,148.0)	2188	(540,212.2)	7842	(0.15, 1110, 275.6)
	318	0.70	100	3571	(15,31.5)	ı	ı	2805	(0.5,180,99.5)	1317	(660,230.7)	4052	(0.31, 1350, 316.3)
_	$318^{A}$	0.50	70	1785	(240,108.1)	ı	ı	5082	(0.32,420,142.6)	2729	(660,208.1)	6042	(0.14,1290,281.1)
	$318^{B}$	0.50	40	1731	(300,101.6)	ı	ı	2164	(0.34,420,123.8)	2155	(600, 178.7)	5727	(0.13,1470,293.7)
0.1M NaCl	318	0.50	100	2467	(180,106.9)	ı	ı	9031	$^{\mathrm{C}}(0.32,300,141.4)$	3176	(780,250.2)	14292	(0.10, 1290, 316.3)
pH=2.8	318	0.50	100	4708	$(30,56.7)^{D}$	2072	(660,223.4)	7156	(0.15,1290,278.3)	ı	ı	ı	1
pH=3.8	318	0.50	100	6836	(60,120.4)	4557	(360,252.2)	9114	(0.13,780,293.3)	ı	ı	ı	ı
pH=12	318	0.50	100	2866	(60,112.9)	ı	ı	12461	$^{E}(0.29,180,178.3)$	5550	(540,229.0)	31450	(0.15,660,273.6)
pH=13	308	0.50	100	1607	(180,107.2)	ı	ı	3638	(0.13,1110,289.4)	ı	ı	ı	1
pH=13	318	0.50	100	2348	(420,168.7)	ı	ı	18820	(0.04,1470,315.7)	ı	ı	ı	1
pH=13	328	0.50	100	4859	(480,263.8)	ı	I	18006	(0.11,930,309.5)	I	I	ı	ı
pH=14	318	0.50	100	ı	(0.36,0.5<,112.2) <sup>F</sup>	3358	(540,194.4)	6427	(0.23,930,216.6)	I	I	ı	I

 $[MnO_4]_{l,mao}^2 t^2$  and  $q_{l,mac}^2$  are  $MnO_4$  concentration, time and adsorption capacity at the end of the adsorption on ME site, respectively (corresponding to  $[MnO_4]_s$ ,  $t_e$  and  $q_e$  on MI site).  $[MnO_4]_s$ ,  $t_e$  and  $q_e$  are  $MnO_4$  concentration, time and adsorption capacity at the beginning of the plateau, respectively. Units of  $k_{11}$ ,  $k_{12a}$  and  $k_{12b}$  are in mg  $g^{-1}M^{-1}$  min<sup>-1</sup>. A and B refer to cases that there were TDs at 4 and 5 min before starting adsorption process, respectively. C, D, E and F refer to TRAKs in the range of 300–360, 60–90, 180–420 and >0.5–180 min, respectively.

Table 6. Non-ideal adsorption acceleration and velocity parameters for the first, second and third curves obtained from the NIPPON equation for kinetics of MnO<sub>4</sub> adsorption on the surface of Co-Al-LDH at 308-328 K

Solvent	T	$[MnO_4^-]_0$	rpm	$(t_e, q_e)$	K	[PPON curve]	rve 1	NIPPON curve 2	curve 2	Z	NIPPON curve 3	
	(K)	(mM)	ı	i	$a_{f_c}^N$	$V_{fc}^{NN}$	$(t_{sc}, q_{sc})$	$a_{sc}^N$	$v_{sc}^N$	$(t_{to} q_{tc})$	$a_{tc}^N$	$V_{tc}^N$
Water	318	0.25	100	(1350,177.7)	-2.7×10 <sup>-2</sup>	1.07	(16,12.6)	-5.9×10 <sup>-2</sup>	1.01	(241,61.1)	-1.2×10 <sup>-3</sup>	0.29
	308	0.50	100	(1470,160.0)	$-4.0 \times 10^{-3}$	0.49	(90,28.3)	$-4.0 \times 10^{-3}$	0.36	(780,100.3)	$-1.6 \times 10^{-4}$	0.12
	318	0.50	100	(1650, 275.6)	$-2.5 \times 10^{-2}$	1.44	(30,31.4)	$-4.7 \times 10^{-2}$	1.45	(300,113.2)	$-1.1 \times 10^{-3}$	0.32
	328	0.50	100	(1110,266.7)	0	1.09	(5,5.5)	-0.38	2.29	(30,27.3)	$-7.6 \times 10^{-2}$	2.35
	318	0.70	100	(1350, 319.3)	-0.25	3.41	(5,12.7)	-0.72	4.29	(180,99.5)	$-3.4 \times 10^{-4}$	90.0
	$318^{A}$	0.50	20	(1290,281.1)	-0.62	3.08	(60,38.9)	$-1.5 \times 10^{-2}$	0.91	(420,142.6)	$-7.3 \times 10^{-4}$	0.31
	$318^{B}$	0.50	40	(1470,293.7)	$-8.8 \times 10^{-3}$	$0.97^{\mathrm{B}}$	(30,21.1)	-0.04	1.29	(420,123.8)	$-7.8 \times 10^{-4}$	0.33
0.1M NaCl	318	0.50	100	(1290,316.3)	-13.89	13.89	(60,58.6)	$-1.4 \times 10^{-2}$	0.88	C(360,141.7)	$-1.0 \times 10^{-3}$	0.38
pH=2.8	318	0.50	100	(1290, 278.3)	0	1.08	(2,2.2)	-2.92	8.77	$^{D}(90,85.7)$	$-8.9 \times 10^{-3}$	0.81
pH=3.8	318	0.50	100	(780,293.3)	-11.32	11.32	(5,20.4)	-1.25	7.50	(90,120.4)	-0.02	1.21
pH=12	318	0.50	100	(660,273.6)	-21.39	21.39	(15,59.6)	-0.20	3.13	E(420,185.4)	$-1.1 \times 10^{-3}$	0.46
pH=13	308	0.50	100	(1110,289.4)	0	1.28	(30,38.2)	$-4.1 \times 10^{-2}$	1.28	(180,170.2)	$-3.5 \times 10^{-3}$	0.64
pH=13	318	0.50	100	(1470,315.7)	-4.35	4.35	(10,10.6)	-0.28	3.11	(180,103.8)	$-3.3 \times 10^{-3}$	0.59
pH=13	328	0.50	100	(930,309.5)	0	68.0	(30,26.8)	-0.10	2.99	I	ı	I
pH=14	318	0.50	100	(930,216.6)	Very fast <sup>F</sup>		(180,110.1)	$-2.2 \times 10^{-3}$	0.41	I	I	ı

A and B refer to cases that there are TDs at 4 and 5 min before starting adsorption process and thus for first curve 1, t = 4 and t = 5 min were used in Eqs. (11) and (12), respectively. C, D, E and F refer to TRAKs in the range of 300–360, 60–90, 180–420 and >0.5–180 min, respectively. Units of  $a_{lc}^{lc}$  and  $a_{lc}^{lc}$  are in mg  $g^{-1}$  min<sup>-2</sup> and those of  $v_{lc}^{lc}$ ,  $v_{cd}^{lc}$  and  $v_{lc}^{lc}$  are in mg  $a_{lc}^{lc}$  and  $a_{lc}^{lc}$  are in min Subscripts fc, sc and tc are abbreviations for starting first curve, starting second curve and starting third curve, respectively and those of  $q_e$ ,  $q_{sc}$  and  $q_{tc}$  are in mg g<sup>-1</sup>.

**Table 7.** Coefficients of the Elovich equation for adsorption of  $\rm MnO_4^-$  adsorption on the surface of ME sites of Co-Al-LDH in various shaking rates and initial  $\rm MnO_4^-$  concentrations and media at  $\rm 308{\text -}328~K$ 

Solvent	Т	[MnO-]	******	~	β	$R^2$
Solvent	(K)	$[MnO_4^-]_0$ $(mM)$	rpm (n	$lpha$ ng g $^{-1}$ min $^-$	,	Л
Water	318	0.25	100	3.11	0.23	0.99
	308	0.50	100	1.16	0.06	0.98
	318	0.50	100	3.88	0.09	0.99
	328	0.50	100	3.67	0.08	0.98
	318	0.70	100	8.33	0.10	0.98
	318A	0.50	70	_	_	_
	318B	0.50	40	_	_	_
0.1M NaCl	318	0.50	100	14.55	0.12	0.99
pH=2.8	318	0.50	100	6.60	0.09	0.99
pH=3.8	318	0.50	100	15.98	0.10	0.99
pH=12	318	0.50	100	29.13	0.05	0.99
pH=13	308	0.50	100	3.56	0.03	0.99
pH=13	318	0.50	100	4.08	0.07	0.92
pH=13	328	0.50	100	3.41	0.014	0.99
pH=14	318	0.50	100	Very i	fast (0.5 mi	n < )

A and B refer to cases that there were TDs at 4 and 5 min before starting adsorption process, respectively.

It was observed that  $k_{I1}$  and  $k_{I2b}$  values in water decreased with a decrease in shaking rate of solution or initial concentration of  $MnO_4^-$ . Also, it should be mentioned that 0.25 mM  $MnO_4^-$  (based on the KASRA model) had only region 1 (or in region I in its related isotherm based on the ARIAN model) and  $MnO_4^-$  ions were adsorbed on the most active adsorption sites without encountering hindrance of adsorbed  $MnO_4^-$  ions. Thus, its  $k_{I1}$  value was greater than  $k_{I1}$  values observed in other tests.

 $k_{I1}$  and  $k_{I2b}$  values in 0.1 M NaCl decreased compared with those in water at 318 K due to competitive adsorption of chloride ion with MnO<sub>4</sub>-

In acidic pHs, because of interaction of H<sup>+</sup> with surface,  $k_{I1}$  and  $k_{I2b}$  values increased with decreasing pH but due to an increase in chloride ion concentration with a decrease in pH from 2 to 1 their values decreased a little.

At pH=11,  $k_{I1}$  value increased a little compared with that in water. This is due to interaction of OH<sup>-</sup> ions with some adsorbent sites that decreased its adsorption capacity. Free MnO<sub>4</sub>-ions encountered less steric hindrance from the small amount of adsorbed ones and this resulted in a little faster interaction of MnO<sub>4</sub>-ions with adsorbent surface at pH=11 compared with that in water.

At pH=12, due to stronger reaction between  $MnO_4^-$  ions and  $MoS_2$  and faster consumption of  $MnO_4^-$  ions,  $k_{I1}$  and  $k_{I2b}$  values in regions 1 and 2 increased drastically compared with those in pH ranges from 1 to 11.

Adsorption kinetics of MnO<sub>4</sub>on MoS<sub>2</sub> were analyzed by NIPPON equation, Table 10. By this analysis, an excess ideal curve was observed at the begining of adsorption kinetic diagrams of 0.5 mM MnO<sub>4</sub> at 308 and 318 K and

 $0.75~\rm mM~MnO_4^-$  at 318 K in water and in 0.5 mM  $MnO_4^-$  in water, 0.1 M NaCl and at pHs of 2 and 11 at 318 K and 100 rpm compared to analysis with the KASRA model. These observations showed that activities of most active adsorption sites located in initial time ranges of first region obtained from the KASRA model were somehow bigger than activities of rest of this kind of adsorption sites.

On the other hand, the NIPPON equation analysis of adsorption kinetic diagrams of 0.25 mM  $\rm MnO_4^-$  at 318, 0.5 mM  $\rm MnO_4^-$  at 328 K, 100 rpm and 0.5 mM  $\rm MnO_4^-$  at 70 and 40 rpm at 318 K and 0.5 mM  $\rm MnO_4^-$  at pHs of 1 and 11 at 318 K and 100 rpm did not show any extra ideal curve at the beginning of them. These observations showed that in these cases the most active adsorption sites of adsorbent in the first region of the KASRA model were similar together.

Analysis of adsorption of  $MnO_4^-$  on adsorption sites of  $MoS_2$  with the Elovich equation showed that  $\alpha$  values changed randomly with an increase in pH, temperature and  $MnO_4^-$  concentration, Table 11.

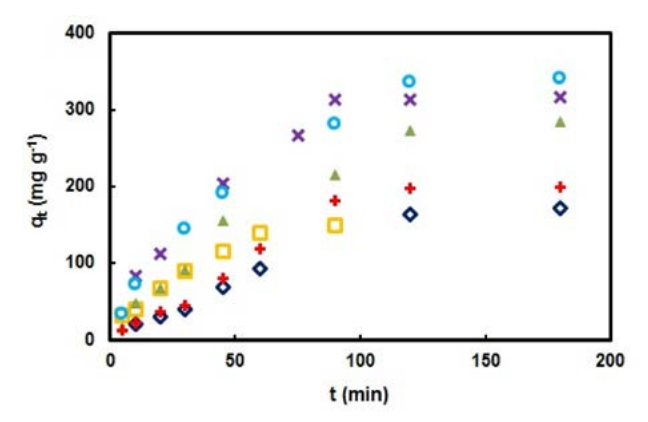


**Fig. 5** Kinetic curves of adsorption of  $MnO_4^-$  on  $MoS_2$  in water in initial  $MnO_4^-$  concentrations of  $\square$  0.25 mM at 318 K, 0.5 mM at  $\clubsuit$  308 K,  $\lozenge$  318 K and  $\times$  328 K and  $\circ$  0.75 mM at 318 K and + 0.5 mM in 0.1 NaCl at 318 K and 100 rpm

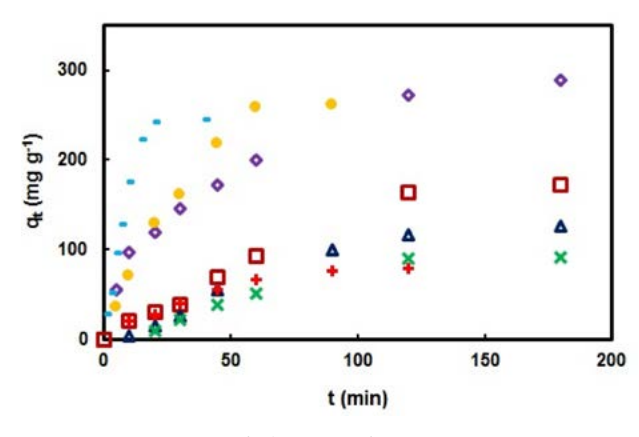


**Fig. 6** Kinetic curves of adsorption of  $MnO_4^-$  on  $MoS_2$  in water in initial  $MnO_4^-$  concentrations of 0.5 mM of  $MnO_4^-$  in  $\square$  water and pHs of  $\lozenge$  1,  $\bullet$  2, + 11 and – 12 and 100 rpm and at  $\times$  40 rpm and  $\Delta$  70 rpm at 318 K

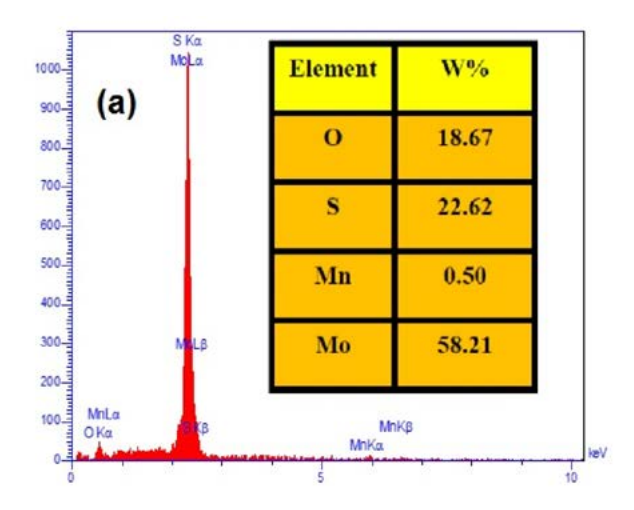
#### 3. 3. 1. Recycling the used MoS<sub>2</sub>

In this work, the used  $MoS_2$  was recycled using a mixture of oxalic and sulfuric acids. In a series of tests, a mixture of 4 ml of 0.1 M oxalic acid and 1 ml of 0.5 M sulfuric acid were added to 0.01 g of the used  $MoS_2$  at room temperature. Mixture was stirred for 10 minutes and the deposited  $MnO_2$  into  $MoS_2$  was reduced to  $Mn^{2+}$  according to the following reaction

$$MnO_{2(ad)} + 4H^{+} + C_{2}O_{4}^{2-} \rightarrow Mn^{2+} + 2CO_{2} + 2H_{2}O$$
 (15)

Comparison of EDS spectra of the initial used  $MoS_2$  sample and recycled  $MoS_2$  showed there was a trace amount of manganese in the product of reaction (15) which verified recycling the used  $MoS_2$  by this reaction, Figs. 7(a) and 7(b).

After three times recycling of the used  $MoS_2$ , the adsorption capacity of the recycled  $MoS_2$  was between 85% and 90% of that of as-synthesized adsorbent.



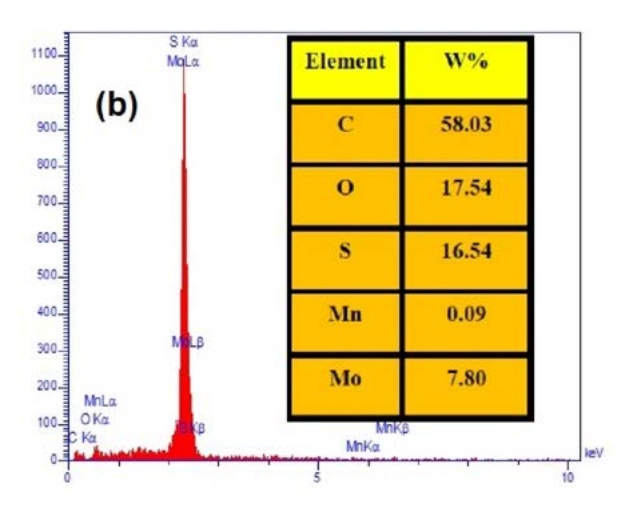


Fig. 7 EDS spectra of a sample of the used  $MoS_2$  (a) before and (b) after recycling by using a mixture of 4 ml of 0.1 M oxalic acid and 1 ml of 0.5 M sulfuric acid solutions

**Table 8.** Experimental  $t_e$ ,  $q_e$ ,  $t_{02}$  and  $q_{02}$  values and coefficients obtained from the KASRA equation and  $k_{dif}$  values of intraparticle diffusion equation for kinetics of MnO<sub>4</sub> adsorption on MoS<sub>2</sub> at different temperatures and in various shaking rates and initial MnO<sub>4</sub> concentrations and media

Solvent	T	$[MnO_4^-]_0$	rpm	$(t_e, q_e)$	KA	SRA regio	on 1		KASRA reg	ion 2	
	(K)	(mM)	-		$a_1$	$v_{01}$	$k_{dif}$	$(t_{02}, q_{02})$	$a_2$	$\nu_{02}$	$k_{dif}$
Correspondi	ing to:				AR	IAN regio	on I		ARIAN reg	ion II	
Water	318	0.25	100	(90,149.6)	-0.04	3.57	21.0	-	_	_	
	308	0.50	100	(180,164.2)	-0.06	2.14	7.0	(30,39.1)	$-2.0\times10^{-2}$	2.41	22.7
	318	0.50	100	(120,273.2)	-0.11	4.67	22.5	(30,91.9)	$-1.2 \times 10^{-2}$	2.51	30.7
	328	0.50	100	(90,313.4)	-0.54	11.0	21.9	(20,119.9)	$-2.2 \times 10^{-2}$	3.56	38.9
	318	0.75	100	(120,335.6)	-0.23	8.34	33.9	(30,145.1)	$-1.2 \times 10^{-2}$	2.72	34.3
	318 <sup>A</sup>	0.50	70	(180,125.5)	-0.05	1.90	8.70	(20,15.0)	$-1.0 \times 10^{-2}$	1.65	15.6
	$318^{B}$	0.50	40	(120,90.1)	-0.006	1.24	12.3		_	_	_
0.1M NaCl	318	0.50	100	(120,196.9)	-0.07	2.52	9.80	(30,44.1)	-0.03	3.25	34.3
pH=1	318	0.50	100	(120,272.0)	-0.72	13.2	27.8	(20,119.6)	$-1.4 \times 10^{-2}$	2.31	23.4
pH=2	318	0.50	100	(60,258.3)	-0.11	7.53	41.8	(20,128,9)	$-2.6 \times 10^{-2}$	3.87	39.8
pH=11	318	0.50	100	(60,76.0)	-0.016	1.57	10.4		_	_	_
pH=12	318	0.50	100	(20,241.5)	0.00	18.0	62.2	(7, 128.3)	-1.27	16.9	62.5

Units of  $a_1$  and  $a_2$  are in mg g<sup>-1</sup> min<sup>-2</sup> and those of  $v_{01}$  and  $v_{02}$  are in mg g<sup>-1</sup>. Units of  $t_e$  and  $t_{02}$  are in min and those of  $q_e$  and  $q_{02}$  are in mg g<sup>-1</sup>. In region 1,  $t_{01}$  and  $q_{01}$  are equal to zero. A and B refer to cases that there are TDs at 7.5 and 10 min before starting adsorption process, respectively.

Table 9. Coefficients of region 1 and region 2 (parts 2a and 2b) of the ISO equation for kinetics of MnO<sub>4</sub> adsorption on MI sites of MoS<sub>2</sub> at 308–328 K

	U	C	.1	,					-
Solvent	T (K)	[MnO <sub>4</sub> ] <sub>0</sub> (mM)	rpm	$k_{I1}$	$(t_{ssr}, q_{ssr})$ (min,mg g <sup>-1</sup> )	$k_{I2a}$	$(t_{sp}, q_{sp})$ (min,mg g <sup>-1</sup> )	$k_{I2b}$	$([\mathrm{MnO_4^-}]_et_e,q_e\ (\mathrm{mM,min,mg}\;\mathrm{g}^{-1})$
	Co	orresponding	to:	ARIA	N region I		A	RIAN reg	ion II
Water	318	0.25	100	27718	-	_	-	_	(0.11,90,149.6)
	308	0.50	100	2287	(30,39.1)	_	_	5363	(0.34,180,164.2)
	318	0.50	100	7623	(30,91.9)	_	_	16517	(0.22, 120, 273.2)
	328	0.50	100	9286	(20,111.9)	_	_	27857	(0.20,90,313.4)
	318	0.75	100	8558	(30,145.1)	_	_	13226	(0.43, 120, 335.6)
	318 <sup>A</sup>	0.50	70	1977	(20,15.0)	_	_	4284	(0.38, 180, 125.5)
	$318^{B}$	0.50	40	1522		_	_	_	(0.42, 120, 90.1)
0.1M NaCl	318	0.50	100	2832	(30,44.1)	_	_	13454	(0.28, 120, 196.9)
pH=1	318	0.50	100	13499	(20,119.6)	_	_	14624	(0.24, 120, 272.0)
pH=2	318	0.50	100	25348	(20.0, 128.9)	_	_	35488	(0.26,60,258.3)
pH=11	318	0.50	100	7993	-	_	_	_	(0.43,60,76.0)
pH=12	318	0.50	100	88376	(7,128.3)	_	_	239706	(0.20, 20, 241.5)
-									

A and B refer to cases that there are TDs at 7.5 and 10 min before starting adsorption process, respectively.  $[MnO_4^-]s$ ,  $t_e$  and  $q_e$  are  $MnO_4^-$  concentration, time and adsorption capacity at the beginning of the plateau respectively. Units of  $k_{I2a}$ , and  $k_{I2b}$  are in mg g<sup>-1</sup> M<sup>-1</sup> min<sup>-1</sup>.

Table 10. Non-ideal adsorption acceleration and velocity parameters for the first, second and third curves obtained from the NIPPON equation for kinetics of  $MnO_4^-$  adsorption on the surface of  $MoS_2$  at 308-328 K

Solvent	T	$[MnO_4^-]_0$	rpm	$(t_e, q_e)$	NIPPO	N curve 1	NIPP	ON curv	e 2	NIPPO	)N curv	re 3
	(K)	(mM)	•	10 10	$a_{fc}^N$	$oldsymbol{v}_{fc}^N$	$(t_{so}, q_{sc})$	$a_{sc}^N$	$v_{sc}^N$	$(t_{tc}, q_{tc})$	$a_{tc}^N$	$v_{tc}^N$
Water	318	0.25	100	(90,149.6)	-17.02	17.02	(10,40.5)	-0.46	5.01	_	_	
	308	0.50	100	(180,164.2)	0	3	(5,15.0)	-1.24	7.4	(30,91.9)	-0.13	3.99
	318	0.50	100	(120,273.2)	0	2.05	(10,20.5)	-0.15	1.61	(30,39.1)	-0.10	2.99
	328	0.50	100	(90,313.4)	-36.1	36.1	(20,111.9)	-0.30	6.27	_	_	_
	318	0.75	100	(120,335.6)	-6.64	6.64	(5,33.2)	-2.10	12.57	(45,191.0)	-0.07	3.18
	318	0.50	70	(180, 125.5)	$-0.21^{A}$	1.76 <sup>A</sup>	(20,15.0)	-0.12	2.56	_	_	_
	318	0.50	40	(120,90.1)	$-0.17^{\mathbf{B}}$	$1.90^{B}$	(30,22.3)	-0.05	1.61	_	_	_
0.1M NaCl	318	0.50	100	(120,196.9)	-2.23	2.23	(10,22.3)	-0.17	1.92	(30,44.1)	-0.12	3.85
pH=1	318	0.50	100	(120,272.0)	-39.6	39.6	(20,119.6)	-0.19	3.97	_	_	_
pH=2	318	0.50	100	(60,258.3)	-7.17	7.17	(5,35.9)	-2.07	12.40	(20,138.9)	-0.28	5.85
pH=11	318	0.50	100	(60,76.0)	-2.76	2.76	(10,27.6)	-0.24	2.62	_	_	_
pH=12	318	0.50	100	(20,241.5)	-36.71	36.71	(3,50.9)	-7.46	29.85	_	_	-

A and B refer to cases that there are TDs at 7.5 and 10 min before starting adsorption process and thus for curve 1, t = 7.5 and t = 10 min were used in Eqs. (11) and (12), respectively. Units of  $a_{fc}^N$   $a_{sc}^N$  and  $a_{tc}^N$  are in mg  $g^{-1}$  min<sup>-2</sup> and those of  $v_{fc}^N$   $v_{sc}^N$  and  $v_{tc}^N$  are in mg  $g^{-1}$  min<sup>-1</sup>. Units of  $t_c$   $t_{sc}$  and  $t_{tc}$  are in min and those of  $q_c$ ,  $q_{sc}$  and  $q_{tc}$  are in mg  $g^{-1}$ . Subscripts fc, sc and tc are abbreviations for starting first curve, starting second curve and starting third curve, respectively.

**Table 11.** Coefficients of the Elovich equation for adsorption of  $MnO_4^-$  adsorption on the surface of  $MoS_2$  in various shaking rates and initial  $MnO_4^-$  concentrations and media at  $308-328~\rm K$ 

Solvent	T (K)	[MnO <sub>4</sub> ] <sub>0</sub> (mM)	rpm	$\alpha$ (mg g <sup>-1</sup> min <sup>-1</sup> )	β (α ma <sup>-1</sup>	$R^2$
	(11)	(1111/1)		(ing g inin )	(g mg	,
Water	318	0.25	100	28.68	0.08	0.96
	308	0.50	100	11.83	0.03	0.98
	318	0.50	100	5.53	0.06	0.98
	328	0.50	100	30.96	0.02	0.99
	318	0.75	100	2.28	0.05	0.98
	318 <sup>A</sup>	0.50	70	_	_	_
	$318^{B}$	0.50	40	_	_	_
0.1M NaCl	318	0.50	100	6.09	0.05	0.99
pH=1	318	0.50	100	30.79	0.02	0.99
pH=2	318	0.50	100	21.73	0.01	0.98
pH=11	318	0.50	100	54.35	0.01	0.99
pH=12	318	0.50	100	5.36	0.06	0.90

A and B refer to cases that there are TDs at 7.5 and 10 min before starting adsorption process, respectively.

#### 4. Conclusions

Reduction of MnO<sub>4</sub> ions to MnO<sub>2</sub> by water molecules was catalyzed after its adsorption on the surface of carbonate intercalated Co-Al-LDH in the pH range of 1-13 and MnO<sub>4</sub> reacted with MoS<sub>2</sub> in the pH range of 1-12. Adsorption kinetic tests were carried out at different temperatures, ionic strengths, pH, initial adsorbate concentrations and shaking rates. The adsorption kinetics was studied by the KASRA model and the KASRA, Elovich, ISO, intraparticle diffusion and NIPPON equations. Results showed that kinetic parameters like  $k_{dif}$ ,  $k_{I1}$ ,  $k_{I2b}$ , adsorption velocities and accelerations of MnO<sub>4</sub> on Co-Al-LDH were increased with an increase in temperature, shaking rate, initial MnO<sub>4</sub> concentration and decrease in pH. But, these parameters at pHs of 12 and 13, due to formation of MnO<sub>4</sub>ions, were less than their values in neutral water and at pH = 14, due to a change in mechanism of reaction, MnO<sub>4</sub>ions reacted with Co<sup>2+</sup> ions of the adsorbent.

However, in the case of  $MoS_2$ ,  $MnO_4^-$  ions were adsorbed on MI sites of  $MoS_2$  and then reacted with it and reduced to  $MnO_2$  in the pH range of 1–12. Study of kinetic curves showed that they were composed from regions 1 and 2 and adsorption velocity and acceleration and  $k_{dij}$ ,  $k_{I1}$  and  $k_{I2b}$  decreased from region 1 to region 2 and in region 1, these parameters increased with an increase in  $MnO_4^-$  initial concentration, temperature, shaking rate and acidic pHs and decreased in 0.1 M NaCl and pH = 11 compared to their values in water. At pH = 12, water molecules were replaced by hydroxide ions and  $MoS_2$  reacted more rapidly with adsorbed  $MnO_4^-$  compared to that in water and changed it to  $MnO_2$ .

 $k_{dif}$ ,  $k_{I1}$  and  $k_{I2b}$  values of adsorption of MnO<sub>4</sub> on MoS<sub>2</sub> were much greater than those for Co-Al-LDH and adsorption of MnO<sub>4</sub> on MoS<sub>2</sub> was very faster than that on Co-Al-LDH.

In this work, the NIPPON equation was introduced. Based on this equation, compared to the KASRA model, an excess curve was observed in the beginning of some adsorption kinetic diagrams that showed some of the most active sites were a little more active than the other ones. Also, in some cases, change in boundary of some curves showed that sites of boundary of some regions are more similar to one of regions. Finally, in this work the used MoS<sub>2</sub> was recycled by using a mixture of oxalic and sulfuric acid solutions.

#### 5. References

- E. Esmaili, B. Samiey, C.H. Cheng, J. Clean. Prod. 2022, 351, 131521. DOI:10.1016/j.jclepro.2022.131521
- S. Ghobadi, B. Samiey, A. Ghanbari, JSSC 2021, 304, 122588.
   DOI:10.1016/j.jssc.2021.122588
- L.P.F. Benício, R.A. Silva, J.A. Lopes, D. Eulálio, R.M.M. dos Santos, L.A. de Aquino, L. Vergütz, R.F. Novais, L.M. da Costa, F.G. Pinto, J. Tronto, Revista Brasileira de Ciência do Solo 2015, 39, 1–13. DOI:10.1590/01000683rbcs2015081
- P. Nalawade, B. Aware, V.J. Kadam, R.S. Hirlekar, JSIR 2009, 68, 267–272.
- S. Velu, K. Suzuki, M.P. Kapoor, S. Tomura, F. Ohashi, T. Osaki, *Chem. Mater.* 2000, *12*, 719–730.
   DOI:10.1021/cm9904685
- Y. Wang, D. Yan, S. El Hankari, Y. Zou, S. Wang, Adv. Sci. 2018, 5, 1800064. DOI:10.1002/advs.201800064
- A.K. Karmakara, Md. Saif Hasanb, A. Sreemanic, A. Das Jayantad, Md. Mehidi Hasane, N.A. Tithef, P. Biswasg, Eur. Phys. J. Plus 2022, 137, 801.
- X. Wan, Y. Song, H. Zhou, M. Shao, Energy Mat. Adv. 2022, 2022, 9842610. DOI:10.34133/2022/9842610
- Z. Tang, Z. Qiu, S. Lu, X. Shi, Nanotechnology Reviews 2020, 9, 800–819. DOI:10.1515/ntrev-2020-0065
- X. Bi, H. Zhang, L. Dou, *Pharmaceutics* **2014**, *6*, 298–332.
   **DOI:**10.3390/pharmaceutics6020298
- L. Shuhui, L. Bin, X. Dawei, L. Yu, C. Fanwei, L. Siqi, J. Chin. Soc. Corros. 2022, 42, 16-24.
- L. Zhang, P. Cai, Z. Wei, T. Liu, J. Yu, A.A. Al-Ghamdi, S. Wageh, J. Colloid Interface Sci. 2021, 588, 637–645.
   DOI:10.1016/j.jcis.2020.11.056
- 13. B.W. Liu, H.B. Zhao, Y.Z. Wang, Adv. Mater. 2021, 2107905.
- D. Kino, Y. Tokudome, P.D. Vaz, C.D. Nunes, M. Takahashi, J. Asian Ceramic Societies 2017, 5, 466–471.
   DOI:10.1016/j.jascer.2017.10.003
- K. Teramura, S. Iguchi, Y. Mizuno, T. Shishido, T. Tanaka, *Angew. Chem. Int.* Ed., **2012**, *51*, 8008–8011.
   DOI:10.1002/anie.201201847
- S. Zhang, J. Chen, W-S Yang, X. Chen, Nano Res. 2022, 15, 7940–7950. DOI:10.1007/s12274-022-4479-z
- N.S. Ahmed, R. Menzel, Y. Wang, A. Garcia-Gallastegui,
   S.M. Bawaked, A.Y. Obaid, Basahel, M. Mokhtar, *JSSC* 2017,
   246, 130-137. DOI:10.1016/j.jssc.2016.11.024
- 18. J. Guo, H. Sun, X. Yuan, L. Jiang, Z. Wu, H. Yu, N. Tang, M.

- Yu, M. Yan, J. Liang, *Water Res.* **2022**, *219*, 118558. **DOI**:10.1016/j.watres.2022.118558
- S. Balendhran, J.Z. Ou, M. Bhaskaran, S. Sriram, S. Ippolito,
   Z. Vasic, E. Kats, S. Bhargava, S. Zhuiykov, K. Kalantar-zadeh, *Nanoscale* 2012, 4, 461–466.
   DOI:10.1039/C1NR10803D
- X. Li, H. Zhu, *Journal of Materiomics* 2015, 1, 33e44.
   DOI:10.1016/j.jmat.2015.03.003
- J. Sun, X. Li, W. Guo, M. Zhao, X. Fan, Y. Dong, C. Xu, J. Deng, Y. Fu, *Crystals* 2017, 7, 198.
   DOI:10.3390/cryst7070198
- X. Gan, H. Zhao, T.W. Lo, K.H.W. Ho, L.Y.S. Lee, D.Y. Lei, K. Wong, ACS Appl. Energy Mater. 2018, 1, 4754–4765.
   DOI:10.1021/acsaem.8b00875
- D. Gupta, V. Chauhan, R. Kumar, *Inorg. Chem. Commun.* 2020, 121, 108200. DOI:10.1016/j.inoche.2020.108200
- R.M.A. Khalil, F. Hussain, A.M. Rana, M. Imran, G. Murtaza, *Nanostruct.* 2019, 106, 338–345.
   DOI:10.1016/j.physe.2018.07.003
- 25. Z. Chen, X. He, C. Xiao, S.H. Kim, *Lubricants* **2018**, *6*, 74. **DOI:**10.3390/lubricants6030074
- K. Lu, J. Liu, X. Dai, L. Zhao, Y. Yang, H. Li, Y. Jiang, RSC Adv. 2022, 12, 798–809. DOI:10.1039/D1RA07962J
- 27. X. Liu, Z. He, S. Xu, J. Wu, J. Wu, Sens. Actuators B: Chem. **2022**, 367, 132185. **DOI:**10.1016/j.snb.2022.132185
- 28. Y. Xiao, J. Yao, T. Zhang, X. Ma, D. Xu, H. Gao, *Dalton Trans.* **2022**, *51*, 638–644. **DOI:**10.1039/D1DT03411A
- A. Kumar, S. Tyagi, R. Kumar, S. Sharma, M. Sharma, R. Adalat, Y. Kumar, R. Chandra, *Mater. Lett.* **2022**, *323*, 132576
   **DOI:**10.1016/j.matlet.2022.132576
- 30. A. Kumar, A. Sood, S.S. Han, *J. Mater. Chem. B* **2022**, *10*, 2761–2780. **DOI**:10.1039/D2TB00131D
- J. Yuan, F. Wang, S. Patel, Z.-L. Hu, M. Tang, J. Lou, ACS Appl. Nano Mater. 2021, 4, 8094–8100
   DOI:10.1021/acsanm.1c01361
- 32. Y. Jia, G. Yin, Y. Lin, Y. Ma, *CrystEngComm* **2022**, *24*, 2314–2326. **DOI:**10.1039/D1CE01439K
- G. Tian, R. Jervis, J. Briscoe, M. Titirici, A.J. Sobrido, *J. Mater. Chem. A* 2022, *10*, 10484–10492.
   DOI:10.1039/D2TA00739H
- Balasubramaniam, S.A. Kumar, K.A. Singh, S.B., Kartikey V.L. Tian, R.K. Gupta, A.K. Gaharwar, *Adv. NanoBiomed Res.* 2022, 2, 2100105. DOI:10.1002/anbr.202100105
- R.A. Street, G.M. Kabera, C. Connolly, S. Afr. Med. J. 2018, 108,187–189. DOI:10.7196/SAMJ.2017.v108i3.12606
- K. Piezer, L. Li, Y. Jeon, A. Kadudula, Y. Seo, *Process Saf. Environ. Prot.* 2021, *148*, 400–414.
   DOI:10.1016/j.psep.2020.09.058
- 37. H. Rahman, *Curr. Anal. Chem.* **2020**, *16*, 670–686. **DOI:**10.2174/1573411015666190617103833
- A. Fawzy, S.A. Ahmed, I.I. Althagafi, M.H. Morad, K.S. Khairou, *Advances in Physical Chemistry* 2016, 2016, 4526578.
   DOI:10.1155/2016/4526578
- E. Geraud, V. Prevot, F. Leroux, J. Phys. Chem. Solids 2006, 67, 903–908. DOI:10.1016/j.jpcs.2006.01.002
- 40. N. Safar Beyranvand, B. Samiey, A. Dadkhah Tehrani, Acta

- Chim. Slov. 2019, 66, 443-454. DOI:10.17344/acsi.2018.4920
- Z. Deng, Y. Hu, D. Ren, S. Lin, H. Jiang, C. Li, Chem. Commun. 2015, 51, 13838–13841. DOI:10.1039/C5CC05069C
- 42. B. Samiey, S. Golestan, *Cent. Eur. J. Chem.* **2010**, *8*, 361–369. **DOI**:10.2478/s11532-009-0135-7
- 43. B. Samiey, S. Abdollahi Jonaghani, J. Pollut. Eff. Con. 2015, 3, 2.
- 44. I. Langmuir, *J. Am. Chem. Soc.* **1918**, *40*, 1361–1403. **DOI:**10.1021/ja02242a004
- 45. M. Boudart, G. Djega-Mariadassou, Kinetics of Heterogeneous Catalytic Reactions, University Press, Princeton, NJ, 1984. **DOI:**10.1515/9781400853335
- M. Rafi, B. Samiey, C.H. Cheng, *Materials* 2018, 11, 496.
   DOI:10.3390/ma11040496
- 47. M. Ozacar, I.A. Şengil, *Colloids Surf. A* **2004**, *242*, 105–113. **DOI:**10.1016/j.colsurfa.2004.03.029
- F-C Wu, R-L Tseng, R-S Juang, Chem. Eng. J. 2009, 150, 366–373. DOI:10.1016/j.cej.2009.01.014
- 49. B. Samiey, S. Farhadi, Acta Chim. Slov. 2013, 60, 763-773.
- B. Samiey, A. Dadkhah Tehrani, J. Chin. Chem. Soc. 2015, 62, 149–162. DOI:10.1002/jccs.201400093
- N. Safar Beyranvand, B. Samiey, A. Dadkhah Tehrani, K. Soleimani, *J. Chem. Eng. Data* 2019, 64, 5558–5570.
   DOI:10.1021/acs.jced.9b00655
- 52. https://en.wikipedia.org/wiki/Fourth,\_fifth,\_and\_sixth\_derivatives\_of\_position
- M. Visser, Class. Quant. Grav. 2004, 21, 2603–2616.
   DOI:10.1088/0264-9381/21/11/006
- 54. S. Lagergren, Handlinger 1898, 24/II, 1-39.
- F. Su, C. Lu, Environ. Sci. Health A 2007, 42, 1543–1552.
   DOI:10.1080/10934520701513381
- A.M. Aljeboree, A.N. Alshirifi, A.F. Alkaim, *Arab. J. Chem.* 2017, 10, S3381–S3393. DOI:10.1016/j.arabjc.2014.01.020
- E.G. Contreras, B.E. Martinez, L.A. Sepúlveda, C.L. Palma, *Adsorp. Sci. Technol.* 2007, 25, 637–646.
   DOI:10.1260/026361707785082396
- 58. S. Karmaker, F. Sintaha, T. Kumar Saha, *Advances in Biological Chemistry* **2019**, *9*, 1–22. **DOI:**10.4236/abc.2019.91001
- U. Geçgel, O. Üner, G. Gökara, Y. Bayrak, Adsorp. Sci. Technol.
   2016, 34, 512–525. DOI:10.1177/0263617416669727
- 60. G. Annadurai, R.S. Juang, D.J. Lee, *J. Hazard. Mater. B* **2002**, 92, 263–274. **DOI:**10.1016/S0304-3894(02)00017-1
- 61. X.S. Hu, R. Liang, G. Sun, *J. Mater. Chem. A* **2018**, *6*, 17612–17624. **DOI:**10.1039/C8TA04722G
- 62. S. Ashour, *J. Saudi Chem. Soc.* **2010**, *14*, 47–53. **DOI:**10.1016/j.jscs.2009.12.008
- 63. L. Soldatkina, M. Zavrichko, *Colloids Interfaces* **2019**, *3*, 4. **DOI:**10.3390/colloids3010004
- 64. K.M. Al-Ahmary, *Int. Res. J. Basic Appl. Sci.* **2013**, 2, 27–37. **DOI**:10.7439/ijpc.v2i4.773
- J.S. Calisto, I.S. Pacheco, L.L. Freitas, L.K. Santana, W.S. Fagundes, F.A. Amaral, S.C. Canobre, *Heliyon* **2019**, *5*, e02553.
   DOI:10.1016/j.heliyon.2019.e02553
- Z. Huang, C. Xiong, L. Ying, W. Wang, S. Wang, J. Ding, J. Lu, *Chem. Eng. J.* 2022, 449, 137722.
   DOI:10.1016/j.cej.2022.137722

- 67. P. Wang, T. Song, C. Xie, P. Yang, *Appl. Surf Sci.* **2022**, *580*, 152290. **DOI:**10.1016/j.apsusc.2021.152290
- A. Kheradmand, M. Negarestani, S. Kazemi, H. Shayesteh, S. Javanshir, H. Ghiasinejad, *Sci. Rep.*, 2022, *12*, 14623.
   DOI:10.1038/s41598-022-19056-0
- H. Cheng, H. He, Z. Zhang, K. Xiao, Y. Liu, X. Kang, X. Li, Sep. Purif. Technol. 2022, 303, 122282.
   DOI:10.1016/j.seppur.2022.122282
- S. Chatterjee, J. Qin, X. Li, F. Liang, D.K. Rai, Y.W. Yang, J. Mater. Chem. B 2020, 8, 2238–2249.
   DOI:10.1039/D0TB00036A
- Y. Zhang, J.R.G. Evans, Colloids Surf. A: Physicochem. Eng. Asp. 2012, 408, 71–78. DOI:10.1016/j.colsurfa.2012.05.033
- S. Verma, C. Mouli Pandey, D. Kumar, New J. Chem. 2022, 46, 21190–21200. DOI:10.1039/D2NJ04285A

- 73. W. Hu, Z. Chang, A. Tang, Y. Wei, D. Fang, X. Lu, P. Shao, H. Shi, K. Yu, X. Luo, L. Yang, *Environ. Res.* 2022, 214, 113969. DOI:10.1016/j.envres.2022.113969
- I. Abouda, S. Walha, S. Bouattour, A.M. Botelhodo Rego, A.M. Ferraria, A.S.C. Sousa, N. Costa, S. Boufi, *J. Environ. Chem. Eng.* 2022, *10*, 108583. DOI:10.1016/j.jece.2022.108583
- 75. W. Zhou, J. Deng, Z. Qin, S. Tong, R. Huang, Y. Wang, *J. Environ. Sci.* **2022**, *111*, 38–50. **DOI:**10.1016/j.jes.2021.02.031
- J.S. Arya Nair, S. Saisree, K.Y. Sandhya, Adv. Sustain. Syst. 2022, 6, 2200039. DOI:10.1002/adsu.202200039
- S. Han, K. Liu, L. Hu, F. Teng, P. Yu, Y. Zhu, Sci. Rep. 2017, 7, 43599. DOI:10.1038/srep43599
- 78. W. Li, Y. Li, Z. Li, Q. Wei, S. Xiao, S. Song, *Minerals* **2018**, *8*, 404. **DOI**:10.3390/min8090404

#### Povzetek

Permanganatni  $MnO_4^-$ ioni so bili adsorbirani na karbonatno interkaliranem Co-Al-slojenem dvojnem hidroksidu (Co-Al-LDH) in  $MoS_2$ . Po določenem času so bili adsorbirani  $MnO_4^-$ ioni reducirani v  $MnO_2$ . Redukcija adsorbiranega  $MnO_4^-$ iona je bila katalizirana na površini karbonatno interkaliranega Co-Al-LDH,  $MnO_4^-$ ioni pa so reagirali s površino  $MoS_2$ . Kinetični testi adsorpcije so bili izvedeni pri različnih temperaturah, ionskih jakostih, pH, začetnih koncentracijah adsorbata in hitrostih stresanja. Adsorpcijsko kinetiko smo preučevali s študijo kinetike adsorpcije v regijah s konstantnim adsorpcijskim pospeškom modela KASRA, študijo idealnega drugega reda (ISO), difuzijo znotraj delcev, Elovich in z enačbo neidealnega procesa adsorpcijske kinetike (NIPPON).

V tem delu je bila predstavljena nova enačba, imenovana NIPPON enačba. V tej enačbi je bilo predpostavljeno, da so bile molekule adsorbatnih vrst med neidealnim procesom adsorbirane hkrati na adsorpcijskih mestih istega tipa z različnimi aktivnostmi. Povprečne vrednosti kinetičnih parametrov adsorpcije so bile izračunane z enačbo NIPPON. S to enačbo je mogoče določiti tudi značaj meja regij, pridobljenih iz modela KASRA.

